JOURNAL OF GEOPHYSICAL RESEARCH, VOL. 114, B01101, doi:10.1029/2007JB005326, 2009

Lithospheric geometry of the Wopmay orogen from a Slave craton to Bear Province magnetotelluric transect

Jessica E. Spratt,[1] Alan G. Jones,[1] Valerie A. Jackson,[2] Louise Collins,[1] and Anna Avdeeva[1]

Received 13 August 2007; revised 8 May 2008; accepted 22 August 2008; published 20 January 2009.

[1] Two-dimensional inversions of lithospheric-probing magnetotelluric (MT) data at a total of 20 sites acquired along an approximately east–west 300-km-long profile across the Wopmay orogen in the Northwest Territories, Canada, provide electrical resistivity models of the boundary between the Archean Slave craton and the adjacent Proterozoic Bear Province. An analysis of distortion effects and structural dimensionality indicates that the MT responses are primarily one-dimensional or only weakly two-dimensional with a depth-independent geoelectric strike angle of N32°E, consistent with regional structural geology. The regional-scale model, generated from the longer period responses from all of the sites along the profile, reveals significant lateral variations in the lithospheric mantle. Resistive cratonic roots are imaged to depths of ~200 km beneath both the Slave craton and the Hottah terrane of the Bear Province. These are separated by a less resistive region beneath the Great Bear magmatic zone, which is speculatively interpreted as a consequence of a decrease in the grain size of olivine in the Wopmay mantle, caused by localized shearing, compared to its neighboring cratonic roots. Focused two-dimensional models, from higher frequency responses at sites on specific sections of the profile, reveal the resistivity structure at crustal depths beneath the region. These suggest that the root of the Slave craton crosses beneath the Wopmay orogen, and that the Wopmay fault zone does not penetrate into the lower crust. A comparison of these results with those obtained during the Lithoprobe project farther south shows striking along strike variations in the conductivity structure associated with the Wopmay orogen.

Citation: Spratt, J. E., A. G. Jones, V. A. Jackson, L. Collins, and A. Avdeeva (2009), Lithospheric geometry of the Wopmay orogen from a Slave craton to Bear Province magnetotelluric transect, *J. Geophys. Res.*, *114*, B01101, doi:10.1029/2007JB005326.

1. Introduction

[2] The Slave craton, in the Northwest Territories of Canada, has experienced in excess of 2.5 billion years of tectonic evolution and provides a unique environment for studying the processes of early Earth development [e.g., *Bleeker*, 2002, 2003; *Davis et al.*, 2003]. Its western boundary provides abundant evident of the accretionary history of the Proterozoic collisional Wopmay orogen that coalesced the Slave craton with the Hottah, Fort Simpson and Nahanni Terranes of the Bear Province (Figure 1). There have been numerous geophysical studies of the Wopmay orogen along its southern boundary as part of the Lithoprobe programme of activities along the SNORCLE transect, but there is no information about the deep lithospheric structure of the orogen along its central part.

[3] In the summer of 2004 magnetotelluric (MT) data were collected along a 300-km-long profile that runs approximately east–west from the western edge of the Archean Slave craton, across the Proterozoic Wopmay orogen, and onto the Phanerozoic platform covering the Proterozoic Bear Province (Figures 1 and 2). The Bear Province comprises four main structural elements (see Figure 1) and extends westward to the MacKenzie Mountains. The main objective of this Slave-to-Bear (S2B) MT study was to define the geoelectric structure, at lithospheric scale, of the Wopmay orogen and the boundary between the Slave craton to the east and the Hottah Terrane to the west. This project was designed to enhance and complement existing geological information and geophysical surveys including MT, seismic reflection, seismic refraction and aeromagnetic data [*Camfield et al.*, 1989; *Cook et al.*, 1998, 1999; *Jones et al.*, 2003; *Lawrence et al.*, 2003; *Fernández-Viejo and Clowes*, 2003; *Clowes et al.*, 2005; *Cook and Erdmer*, 2005; *Wu et al.*, 2005]. The MT data collected along this profile provide information on the crustal structure and mantle properties beneath the region, with the view to constraining the tectonic evolution of the area.

[4] By revealing the electrical resistivity structure of the subsurface, the MT method has proven to be a useful tool in unraveling the complex structure and tectonic history of other Precambrian collisional orogens, such as the Trans-Hudson orogen and the Snowbird tectonic zone [*Jones and Craven*, 1990; *Jones et al.*, 2002, 2005; *Evans et al.*, 2005]. The most commonly proposed causes for enhanced conductivity (reduced resistivity) in the crust include graphite

[1]Dublin Institute for Advanced Studies, Dublin, Ireland.
[2]NWT Geoscience Office, Yellowknife, Northwest Territories, Canada.

0148-0227/09/2007JB005326$09.00

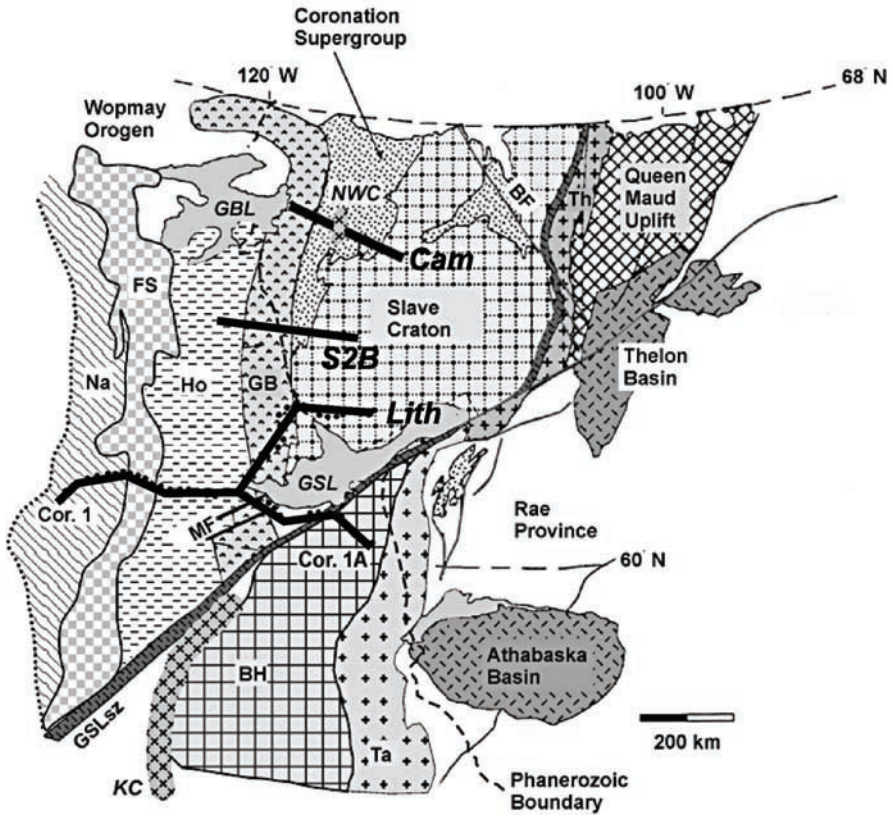

Figure 1. Tectonic elements of the northwest Canadian Shield [after *Hanmer*, 1988] and EM surveys. *Cam*, location of the GDS survey by *Camfield et al.* [1989]; *S2B*, Slave-to-Bear MT profile discussed herein; *Lith*, Lithoprobe profiles along Corridors 1 and 1A discussed by *Wu et al.* [2002, 2005]. The SE–NW broken line marks the eastern margin of the Phanerozoic sedimentary cover. Tectonic units: BF, Bathurst fault zone; BH, Buffalo Head terrane; FS, Fort Simpson terrane; GB, Great Bear magmatic arc; GSLsz, Great Slave Lake shear zone; Ho, Hottah terrane; MF, McDonald fault system; Na, Nahanni terrane; SC, Slave craton; Ta, Talston magmatic zone; Th, Thelon magmatic zone. Geographic features: GBL, Great Bear Lake; GSL, Great Slave Lake. Electrical features: KC, Kiskatinaw Conductor; NWC, Northern Wopmay Conductor.

or thin carbon films, fluids (derived from either metamorphic brine or partial melting), sulfides, interconnected metallic minerals, or a combination of these [*Haak and Hutton*, 1986; *Jones*, 1992; *Duba et al.*, 1994]. The MT method can identify the presence or absence of conductive anomalies in the mantle, as well as define the thickness of the lithosphere [*Jones*, 1999], but the causes for conductivity variations in the lithospheric mantle are still under debate (see below), although clearly for Paleoproterozoic orogens one can exclude saline fluids with confidence given residence-time arguments. Armed with the geometry of the conductive structures revealed and likely candidates for enhancing conductivity, one can provide important information on the tectonic evolution of the region.

2. Geological Setting and Geophysical Background

2.1. Geology and Tectonics

[5] The Slave Province is a small craton in northwestern Canada that contains the oldest rocks in the world and forms part of the Precambrian continental core of North America. Its cratonic assembly was complete by ca. 2.55 Ga [*Bleeker*, 2002; *Davis et al.*, 2003], subsequent to which Proterozoic terranes were accreted to its margins [*Hildebrand and Bowring*, 1987]. The Slave craton was built upon two basement components; a western and central Mesoarchean (4.0–2.9 Ga) basement, that is referred to as the Central Slave Basement Complex [*Bleeker et al.*, 1999a, 1999b], and an eastern, younger (<2.85 Ga), undefined (island-arc?) basement [*Thorpe et al.*, 1992; *Davis and Hegner*, 1992; *Davis et al.*, 1996]. Deposition of a thin cover sequence on the Central Slave Basement Complex was followed by extensive tholeiitic volcanism, widespread calc-alkaline volcanism and finally the deposition of thick turbidite sequences [*Ootes and Pierce*, 2005; *Jackson*, 2006]. The basement complexes and supracrustal sequences were invaded by Neoarchean intrusions. The most eastern point of the MT profile discussed herein lies within the western part of the Central Slave Basement Complex and traverses westward, through an area of potential juvenile crust that lacks evidence of basement [*Davis and Bleeker*, 1999; *Bleeker et al.*, 1999a, 1999b; *Bennett et al.*, 2005], and off the exposed Slave craton onto rocks of the Wopmay orogen.

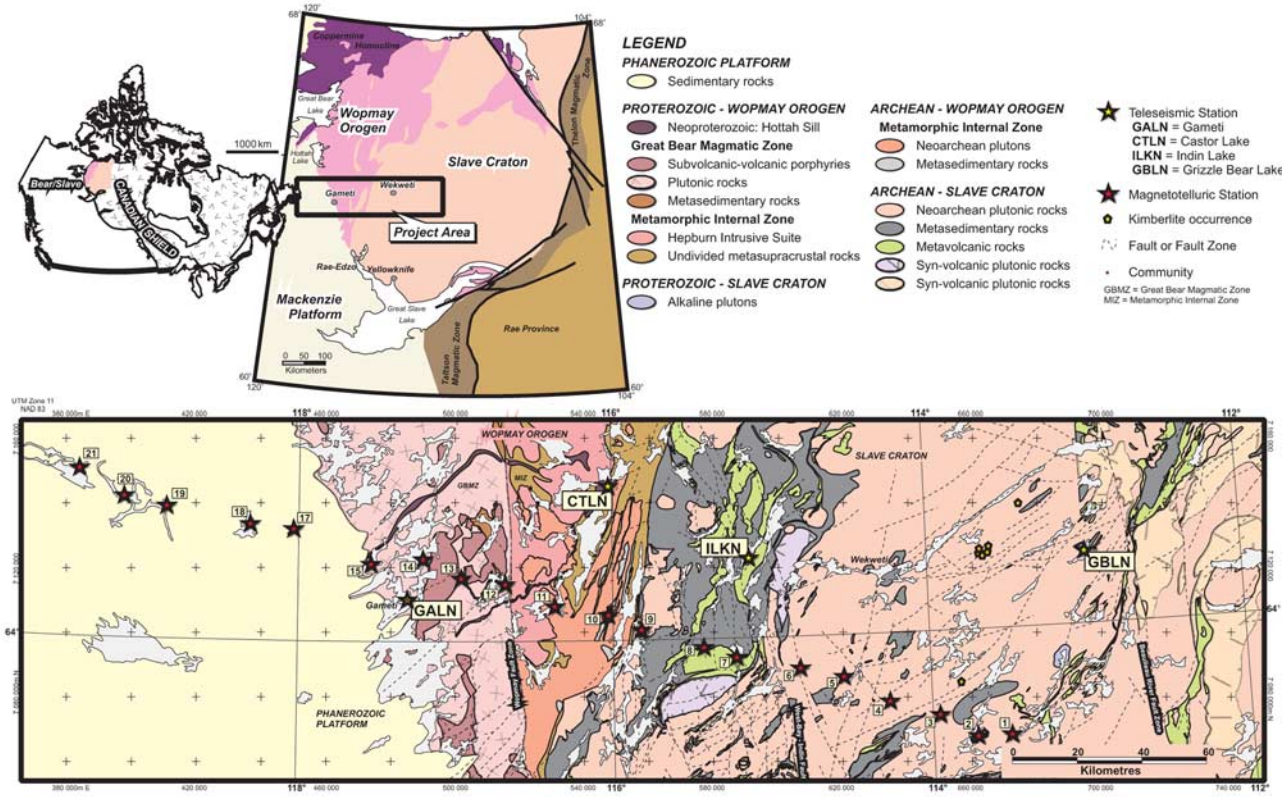

Figure 2. Geology and location map for the MT profile across the western Slave craton and the Wopmay orogen in the Northwest Territories, Canada. Geology is based on *Hoffman and Hall* [1993], *Pierce and Turner* [2004], *Stubley* [2005], and *Jackson* [2006]. GALN, CTLN, ILKN, and GBLN are POLARIS seismic stations of *Snyder and Bruneton* [2007].

[6] The Paleoproterozoic, north-trending Wopmay orogen of the Bear Province developed as the west margin of the Slave craton rifted and subsequently collided with a cryptic microcontinent – the Hottah terrane – during eastward directed subduction [*Bowring and Grotzinger*, 1992]. The orogen can be subdivided from east to west into the following major tectonic elements; the continental margin sedimentary prism, the Wopmay fault zone, the Great Bear magmatic zone, and the Hottah terrane (Figures 1 and 2).

[7] The passive margin sequence along the western Slave craton developed between ca. 1970 and 1890 Ma on rocks of the Slave craton [*Hoffman and Bowring*, 1984]. More westerly strata were invaded by a diverse suite of plutons and were thrust eastward toward the craton and, in northern parts of the orogen, an extensive fold and thrust belt is preserved.

[8] The Great Bear magmatic zone, the youngest tectonic element in the Wopmay orogen, comprises volcano-sedimentary sequences and plutonic rocks with calc-alkaline affinity that record arc magmatism from ca. 1875 Ma to 1840 Ma. Rocks of the magmatic zone were deposited on and intruded into the Hottah terrane and the Slave craton [*Hildebrand and Bowring*, 1987, Figures 1 and 2]. At the Slave craton's southern boundary, along Lithoprobe's SNORCLE transect Corridor 1 (Figure 1), *Cook et al.* [1998] interpret the magmatic zone to result from eastward subduction (in present day coordinates) of oceanic lithosphere beneath the western edge of the Hottah terrane. Interpretations of seismic reflection results show the magmatic arc to form a thin basin (3.0–4.5 km thick) overlying the transition between the Hottah terrane and the Slave craton [*Cook et al.*, 1998].

[9] The poorly understood Hottah terrane forms the westernmost tectonic element of Wopmay orogen and consists of the Hottah arc, a suite of ca. 1936 Ma to 1890 Ma plutons [*Bowring*, 1985] that intruded an ill-defined, variably metamorphosed sequence of sedimentary and volcanic rocks. The Hottah arc is interpreted to have evolved upon an isotopically defined 2.0–2.4 Ga crust [*Housh et al.*, 1989], for which there is no known bedrock exposure. *Hildebrand and Bowring* [1987] and *Bowring and Podosek* [1989] interpret the Hottah terrane to extend eastward beneath much of the Great Bear magmatic zone (Figure 3). As a result of collapse of the ocean basin off the western Slave craton, and possibly the initiation of westward-directed subduction beneath the Hottah terrane, some of the Hottah rocks and the Coronation Supergroup rocks were thrust toward the western edge of the Slave craton forming an intracrustal cratonic wedge (Figure 3) [*Bowring and Grotzinger*, 1992; *Cook et al.*, 1999].

[10] The north-striking Wopmay fault zone is a prominent linear feature that dissects the Wopmay orogen. It has been interpreted as the surface expression of a suture between the Hottah terrane to the west and the Slave craton to the east [*Bowring and Podosek*, 1989]. No exposures of Archean rocks have been mapped west of the Wopmay fault zone

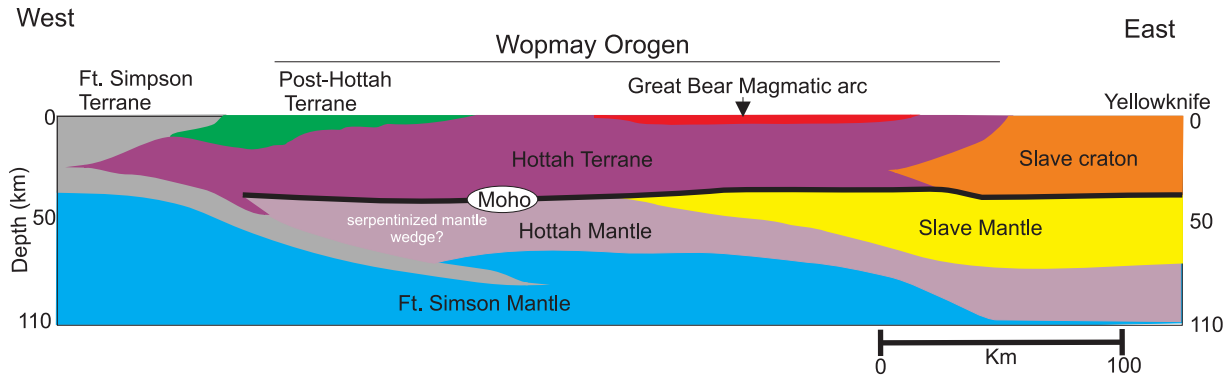

Figure 3. Cross-section model along the SNORCLE seismic profile at approximately 62° latitude west of Yellowknife. Based on *Cook et al.* [1998].

[*Hildebrand et al.*, 1990; *Jackson*, 2006]. In addition, isotopic studies in the northern parts of Wopmay orogen concluded that there is no evidence of Archean crust west of the fault zone [*Bowring and Podosek*, 1989; *Housh et al.*, 1989]. The western extent of the lithosphere of the Slave craton is still under debate, and is one of the over-arching targets of the present study.

[11] The extreme western part of the MT profile crosses from the Canadian Shield into the flat lying to gently west-dipping Paleozoic rocks of the Interior Platform. These strata, possibly Ordovician in age [*Fraser*, 1967], blanket rocks of the Great Bear magmatic zone and the Hottah terrane. Using aeromagnetic maps the western limit of the Proterozoic rocks of Wopmay orogen beneath this cover can been interpreted to extend over 200 km to the west of the Paleozoic-Proterozoic contact [*Lawrence et al.*, 2003].

2.2. Geophysical Results and Previous MT Surveys

[12] The Geomagnetic Depth Sounding (GDS) data from a late-1970s survey by *Camfield et al.* [1989] (profile *Cam* on Figure 1) were dominated by a conductive feature, named the Northern Wopmay Conductor (NWC) and modeled as an upper crustal 50-km-wide body of thickness 1.5 km and resistivity 20 ohm m, that correlates spatially with graphitic pelites of the Odjick Formation, a slope-rise facies. *Boerner et al.* [1996] suggested that the conductor resulted from foredeep facies rocks, specifically euxinic shales of the Fontano Formation.

[13] As part of the Lithoprobe project, several MT surveys have taken place within the Slave craton and have revealed a number of important features. A low-resistivity zone, the Central Slave mantle conductor, underlies the central part of the Slave craton and is co-located with the diamondiferous Eocene-aged kimberlites and a shallow ultra-depleted lithospheric layer [*Jones et al.*, 2001, 2003]. It was also shown that the base of the electrical lithosphere is deeper, at 260 km, beneath the southern third of the Slave craton compared to the central third that has a thickness of around 200 km [*Jones et al.*, 2003]. These electrically defined lithospheric thicknesses for the southern and central Slave craton are consistent with petrologically defined ones from *Pearson et al.* [1999] for the central Slave and *Kopylova and Caro* [2004] for the southern Slave craton. Finally, beneath the Central Slave Basement Complex, in the southwest corner of the Slave craton, there is an anomalously resistive crust and upper mantle, limiting the extent of the Central Slave mantle conductor [*Jones and Ferguson*, 2001].

[14] On the basis of the position of the Central Slave mantle conductor, as well as current geophysical, geological and geochemical information, it has been suggested that the lithospheric mantle beneath the Slave craton was formed by subcreting Mesoarchean lithosphere from the southeast [*Davis et al.*, 2003]. This tectonic model is supported by the teleseismic studies that indicate layering at lithospheric depths, as well as the seismic reflection results interpreted as evidence of subcretion of Paleoproterozoic lithosphere beneath the western Slave craton [*Cook et al.*, 1999; *Snyder et al.*, 2003]. *Snyder* [2008] recently modified the model of *Davis et al.* [2003] and suggested that northwest subduction from the southeast was followed by southeast subduction from the northwest, primarily based on the ages of granites.

[15] Also as part of the Lithoprobe project, magnetotelluric data were collected across the Wopmay orogen along a profile extending from the southwestern margin of the Slave craton [*Wu et al.*, 2005]. The geoelectric strike direction in the crust was determined to be N34°E, and was interpreted to be controlled by transcurrent faulting throughout the region. Two-dimensional modeling of these data indicate resistivity variations associated with the Wopmay orogen, including a prominent conductive zone (<100 ohm m) at the western edge of the Hottah terrane, as well as a region of enhanced conductivity (<10 ohm m) at mantle depths (60–80 km) beneath the Hottah terrane and Great Bear magmatic arc. *Wu et al.* [2005] interpreted this mantle conductive zone to be caused by the presence of interconnected graphite or sulfides that were introduced during subduction prior to the collision between the Hottah terrane and the Slave craton.

[16] Seismic reflection data suggest that lower crustal Hottah rocks were emplaced in the mantle during subduction [*Cook et al.*, 1998]. *Cook et al.* [1999] show mantle reflections located at depths of about 82 km near the transition between the Hottah terrane and the Slave craton, and interpret these reflections as either a flat subduction zone or a preserved mantle fault. The presence of a low-velocity, upper mantle region beneath the western Hottah terrane is interpreted to be caused by serpentinization of mantle peridotite by water derived from a subducting slab [*Fernández-Viejo and Clowes*, 2003].

3. MT Theory and Data Analysis

[17] The magnetotelluric method (MT) is a geophysical exploration technique that provides information on the three-dimensional electrical conductivity of the subsurface of the Earth by measuring and relating the natural time-varying horizontal electric (E) and magnetic (H) fields at its surface [*Cagniard*, 1953; *Wait*, 1962; *Jones*, 1992]. The measurement of these mutually perpendicular electric and magnetic fields allows us to calculate magnitudes (scaled as apparent resistivities) and phase lags at various frequencies, known as MT response curves, for each MT site recorded. Since the depth of penetration (or skin depth) of these fields is dependent on frequency (the lower the frequency, the greater the depth) and the conductivity of the material (the lower the conductivity, the greater the depth), estimates of depth can be made from the response curves beneath each site [*Jones*, 1983].

[18] In a two-dimensional Earth, where the conductivity varies laterally along a profile and with depth, the apparent resistivities and phases are different along strike (parallel to geoelectric strike) than in the perpendicular direction, and both modes need to be calculated [*d'Erceville and Kunetz*, 1962; *Rankin*, 1962]. The transverse-electric (TE) mode refers to the direction parallel to geo-electric strike, and the transverse-magnetic (TM) mode perpendicular to strike. When the Earth is one-dimensional, i.e., layered, these two modes show exactly the same phases (apart from a 180° phase difference) and apparent resistivities. Where the Earth is two-dimensional, some form of directionality analysis needs to be undertaken to determine the preferred geoelectric strike direction consistent with the data. The most powerful approach is that of *Groom and Bailey* [1989], which determines the strike direction statistically as well as mathematically describing the effects of galvanic distortions and three-dimensionality. The results of decomposition analyses provide the TE and TM mode response curves that most accurately represent the two-dimensional regional structure beneath a profile, and present a statistical understanding of the error, distortion and dimensionality in the data.

3.1. Data Acquisition

[19] The magnetotelluric profile consists of twenty broadband (BBMT) MT sites and six long-period (LMT) MT sites merged with every fourth BBMT site. These sites were installed at approximately 20 km intervals next to lakes that were large and deep enough for deployment by float plane (Figure 2) for access reasons. Unfortunately we obtained no usable data from Site 016 because of local fauna (bears) repeatedly damaging the installation. Each MT site comprised five Pb-PbCl (lead-lead-chloride) electrodes laid out in a cross, which measure the electric field of the Earth, a 3-component magnetometer (LMT) or 2 separate magnetometer coils (BBMT), to measure the magnetic field of the Earth, and a recording box. Solar panels and 12V, 85 Ahr batteries were used to power the recording units for the required length of acquisition time.

[20] The BBMT sites used MTU-5A recording boxes and MTC-50 induction coils owned by the Geological Survey of Canada and built by Phoenix Geophysics, and recorded data in the period range of 0.004 to 1000 s for two days. Each of these BBMT sites measured the two horizontal, perpendicular magnetic field components (Hx and Hy). The vertical magnetic field component (Hz) was not recorded because of the logistical problems of installing the vertical coil in frozen ground, extensive throughout the region.

[21] The long-period sites, numbers 001, 005, 009, 013, 017, and 021, used LiMS recording instruments designed and owned by the Geological Survey of Canada [*Anderson et al.*, 1988] and 3-component ring-core fluxgate magnetometers [*Narod and Bennest*, 1990] that were oriented (magnetic) northwards. These sites recorded data at a 5 second sampling rate for 3–4 weeks in the period range of 10–30,000 s. Therefore the total period range at every fourth site was between 0.004 and 30,000 s. Service checks on the long-period sites were performed every 10 days in order to verify the status of data acquisition and to the check for potential problems with the site and the recorded time series.

3.2. Data Processing

[22] Modern processing techniques were applied to these data to ensure that the most accurate and realistic MT response curves were produced to the longest period possible for each site. These techniques included inspection of the time series, processing using robust remote referencing codes, based on *Jones and Jödicke* [1984], for the LMT data and Jones-based Phoenix codes for the BBMT data, as well as analysis of auroral effects, distortion, and geoelectric strike direction [*Groom and Bailey*, 1989; *Jones and Spratt*, 2001; *McNeice and Jones*, 2001].

[23] After visual inspection of the time series and removal of large sections of bad or null data, MT response curves were generated for each site along the profile. For the long-period data, apparent resistivity and phase curves in two perpendicular directions, as well as the vertical field transfer function response estimates, were generated for each site using the multi-remote-reference, robust, cascade decimation code of Jones [*Jones and Jödicke*, 1984] (method 6 in *Jones et al.* [1989]). The BBMT data were processed using remote-referencing Phoenix processing software, which is based on *Jones and Jödicke* [1984]. The long-period response curves (LMT curves) were then merged with the BBMT curves to obtain apparent resistivity and phase estimates in the period range of 0.004–30,000 s. Due to the high latitude of the acquired data set, the data were analyzed for distortion effects resulting from the auroral electrojet [*Mareschal*, 1986], using the method described in *Jones and Spratt* [2001]. This analysis showed some improvement (more reasonable curves) at the very long periods for some sites, providing more reliable estimates of the deep structure beneath the profile.

[24] For most of the sites along the profile the data are of good quality to at least 1000 s (examples in Figures 4A–4D). Unfortunately, due to continual animal disturbances, where LMT data were acquired there was no significant improvement in the long-period responses. For some of the sites the responses were extended out to 2000–3000 s (e.g., site 001, Figure 4D), but for others we discarded the LMT responses.

[25] Schmucker's C-function conversion [*Schmucker*, 1970] was applied to the data from each site to estimate the maximum depth of penetration. This approach is based on 1-D estimation methods, and is also valid when the two 2-D modes, TE and TM, are totally decoupled [*Jones*,

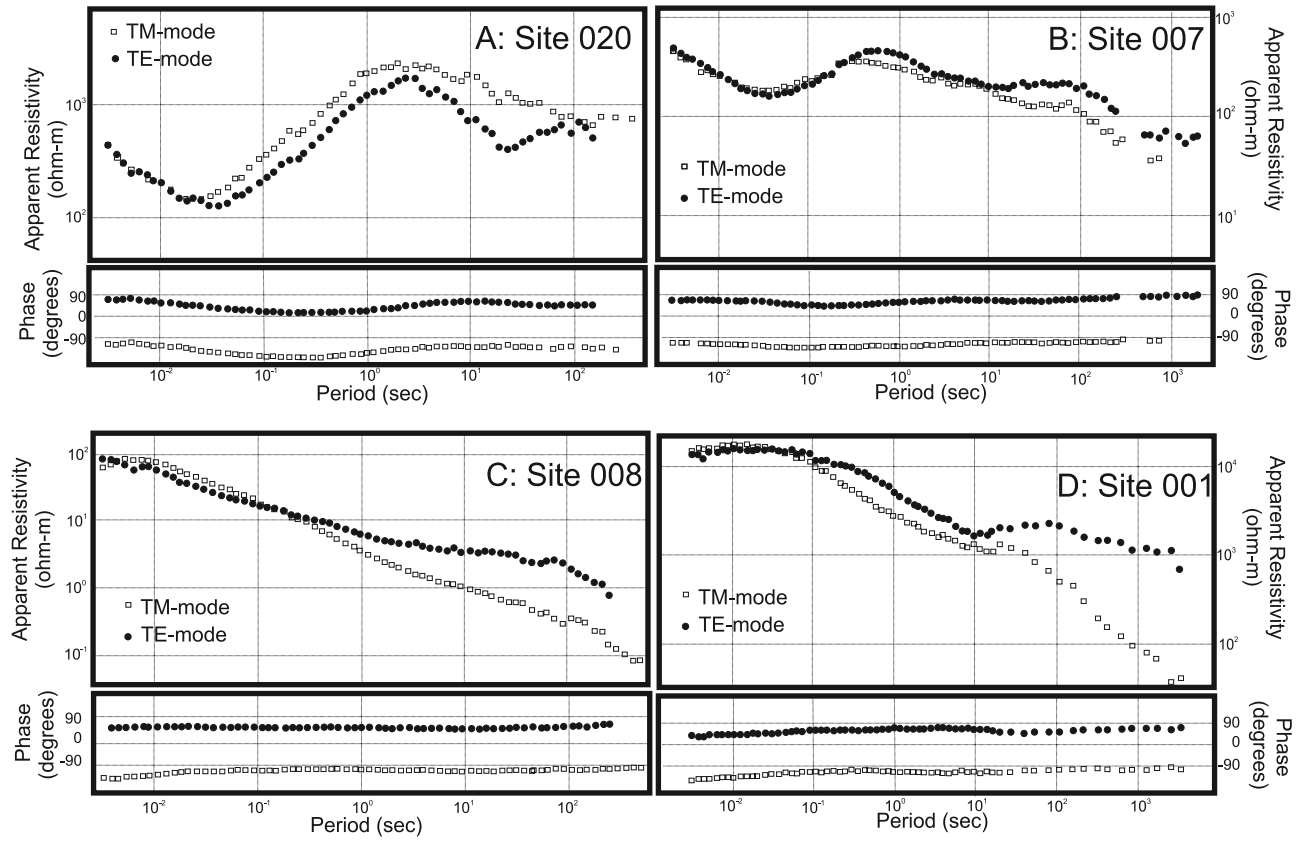

Figure 4. Response curves, apparent resistivity, and phase plotted against increasing periods, calculated for four sites along the MT profile: (A) data from the western end of the profile, site 020; (B) data from site 007; (C) data from site 008; and (D) data from the eastern end of the profile, site 001. The open squares show the transverse-magnetic (TM) mode data, and the solid circles show the transverse-electric (TE) mode data.

2006]. More sophisticated approaches, e.g., *Solon et al.* [2005], confirmed that this approximation provides reasonable estimates of depth penetration. These depth estimated infer that there is a sufficient penetration (>150 km) at most sites along the profile to model lithospheric mantle features (see red bars in Figure 7). Site 008 is an exception where the maximum depth of penetration was calculated to be <4 km. The response curves for this site show the apparent resistivities dropping steeply with increasing period (Figure 4C). This indicates the presence of an anomalously conducting body at very shallow depths beneath site 008, which the fields at the lowest frequencies do not penetrate through and are arrested in the conductive anomaly. Although the neighboring site, 007, does indicate the presence of a shallow conductor, the apparent resistivities begin to rise with increasing periods indicating that the fields are able to penetrate beyond the base of the conductor (Figure 4B).

3.3. Decomposition Analysis

[26] The distortion decomposition code developed by *McNeice and Jones* [2001] was used on the MT response estimates for each of the MT sites along the profile to analyze for galvanic distortions and to determine the most consistent geoelectric strike direction. This 3-D/2-D distortion model assumes that the regional structure is two-dimensional but that the electric field data are galvanically distorted by three-dimensional local near-surface features.

[27] The strike azimuth and the average phase difference between the conductive and resistive directions from single site, one-decade bandwidth, decompositions are shown in Figure 5 for period bands between 0.01–1000 s. Most of the sites along the profile show a fairly one-dimensional response, that is where there is little phase difference between the TM and TE modes, with the exception of a group of five sites, 010 to 014 (Figure 5), and of site 005 (Table 1). There is little evidence of period-dependent geoelectric strike variation, which infers there is little depth-dependent strike variation and thus no evidence for crust-mantle decoupling.

[28] Multi-site decompositions, analysis of galvanic distortion parameters twist and shear, and observations of the (RMS) misfit consistently yielded a preferred geoelectric strike azimuth of approximately N32°E that was found to best-fit most of the sites along the profile at most of the frequencies, and this geoelectric strike was adopted for further analysis. The distortion decomposition parameters in this constrained strike angle, and for frequency-constrained galvanic distortion parameters twist and shear, are given in Table 1. Also listed is the average phase difference at periods shorter and longer than 10 s, and the overall average RMS misfit of the distortion model to the data for all periods, and for periods shorter and longer than 10 s. This period is chosen as it is approximately the

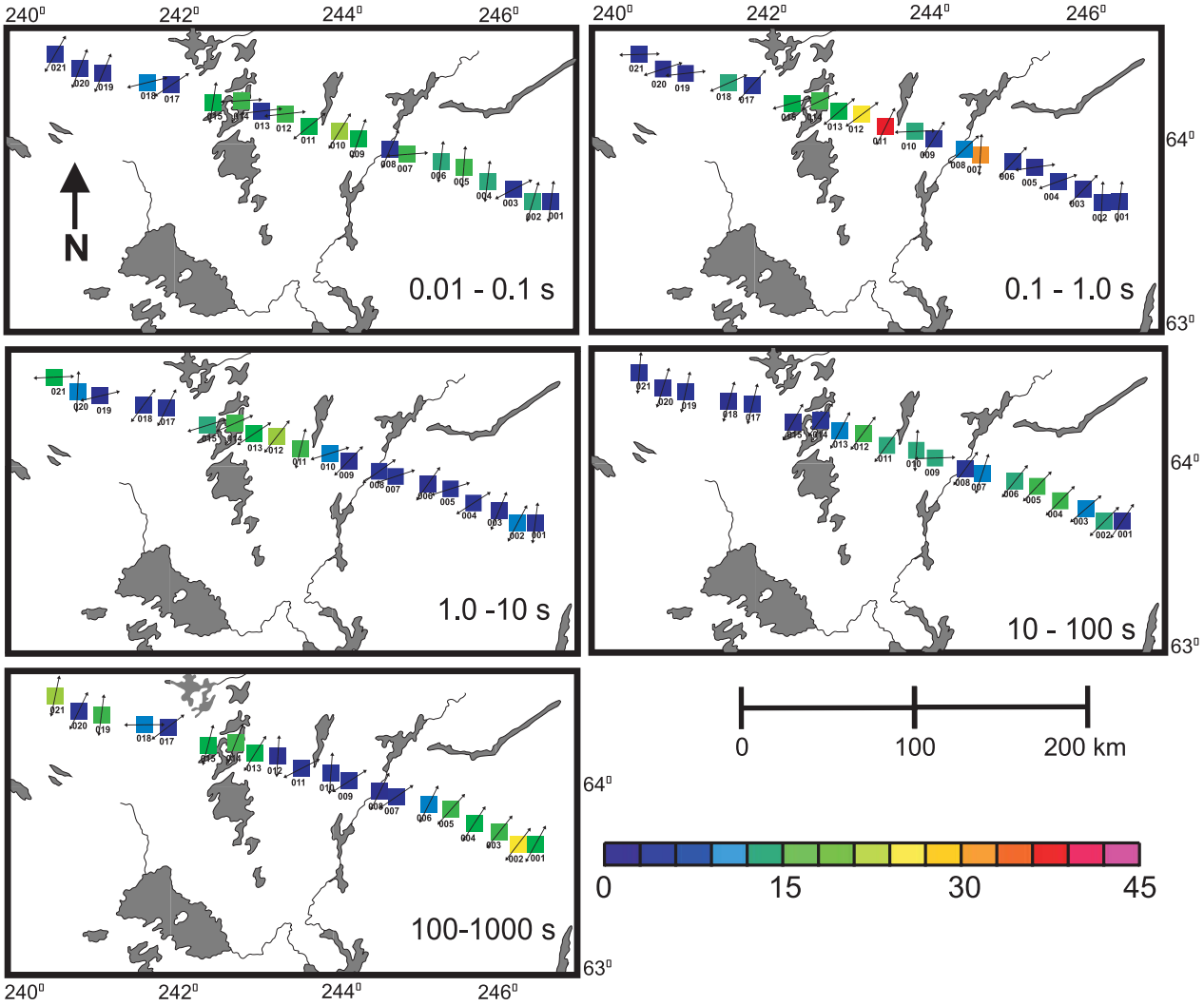

Figure 5. The strike angle determined from Groom-Bailey decompositions is shown for each site at three different period bands at increasing depths in the Earth. The color represents the maximum phase difference between the TM and TE modes.

period for EM waves sensing the crust-mantle boundary [see, e.g., *Wu et al.*, 2002; *Eaton et al.*, 2004], so the shorter periods are representative of crustal structures and the longer periods of mantle structures.

[29] The 3-D/2-D galvanic distortion model fits the data well within an acceptable RMS of below 1.00 at almost all sites and for almost all periods (Table 1). The main exceptions are for responses in the period band 0.1–1.0 s, where the misfit at some sites is 2.0 to 3.0. However, this can be attributed to the overly optimistic error estimates at those periods derived using the parametric error estimator in Phoenix's codes. Comparisons with non-parametric jackknife error estimators demonstrate that the parametric error estimates are too small, typically by factors of 3–5, when the number of estimates is high [*Chave and Jones*, 1997].

[30] There is strong distortion at many sites, as shown by the large values of shear (physically maximum value of 45°), but at most sites the phase difference between the orthogonal directions is well below 15°, especially for "crustal" periods. Certainly the sites at the western end of the profile, 015 to 020, can be treated as 1-D, and, with the exception of sites 010 to 014 and site 005, the crust can be treated as 1-D. The rest of the data are weakly two-dimensional.

[31] This strike angle of N32°E is consistent with Proterozoic faulting in the western half of the profile, therefore the TE mode (transverse electric) was designated to run parallel these faults (N32°E), and the TM mode (transverse magnetic) to run perpendicular to the geoelectric strike angle (N58°W). Induction vectors, derived from the vertical and horizontal magnetic fields at the three long-period eastern sites 001, 005, 009 (see Table 2), are low in amplitude and display scatter, indicative of predominantly 1-D structure below and likely influenced by residual effects from the non-uniform source fields [see *Jones and Spratt*, 2001]. The vectors from the western three sites, 013, 017 and 021, are less scattered and are higher in amplitude (Table 2). The reversed real induction arrows at these sites point N30°W to N45°W at the period of maximum amplitude (215 s), supporting this designation for the TE- and TM modes.

Table 1. Constrained Distortion Decomposition Values for a Geoelectric Strike of N32°E[a]

Station	Shear at 32°	Twist at 32°	Average Phase Difference at 32° for Periods <10 s	Average Phase Difference at 32° for Periods >10 s	Average RMS Misfit at 32°	Strike Range of Average RMS < 1.0: All Periods	Strike Range of Average RMS < 1.0: Periods <10 s	Strike Range of Average RMS < 1.0: Periods >10 s
001	−29.4	−31.4	6.2	16.8	0.85	25–51	0–90	27–36
002	12.2	−8.3	8.1	17.7	0.74	0–90	−7–32	0–90
003	−10.0	3.1	3.6	11.9	0.37	0–90	0–90	0–90
004	32.1	0.2	5.0	19.6	0.55	0–90	0–90	0–90
005	33.8	31.6	28.9	32.9	0.96	32–85	0–90	27–61
006	32.9	−27.8	8.4	17.9	0.26	0–90	−7–71	0–90
007	−36.8	−2.6	4.1	7.4	0.95	−9–42	−7–12	0–90
008	17.4	−17.3	11.0	8.3	1.81	*	*	0–90
009	36.0	17.3	6.0	18.0	0.82	0–90	0–90	28–99
010	−23.3	−11.5	14.7	15.4	0.36	0–90	0–90	0–90
011	−12.4	−3.1	18.9	13.8	0.89	23–38	*	0–90
012	38.7	8.7	13.5	13.5	0.75	17–66	38–60	0–90
013	32.4	23.9	34.6	15.0	1.22	*	37–92	24–40
014	38.9	22.4	23.6	12.7	0.65	12–91	29–91	0–90
015	3.7	−6.2	6.9	11.5	1.10	*	−27–10	0–90
017	−32.9	−6.8	3.6	7.7	0.59	0–90	0–90	9–31
018	−14.2	−0.4	3.9	4.4	0.40	0–90	0–90	0–90
019	−11.9	−0.9	2.0	6.1	0.60	0–90	0–90	0–90
020	−16.0	−2.9	3.9	8.1	0.18	0–90	0–90	0–90
021	−32.9	−29.0	12.8	12.8	1.08	*	0–90	*

[a]Shear and Twist are descriptors of the strength of galvanic distortion, the average phase differences between orthogonal directions (N32°E and N58°W) at periods shorter and longer than 10 s (approximate period to reach the base of the crust), the average RMS misfit of the distortion model to the data, and the range of strike angles that are an acceptable fit (average RMS < 1.00) for all periods, for those shorter and longer than 10 s (* indicates that no strike angles are found with an average RMS < 1.00).

[32] Single-site, frequency-independent decompositions were then performed on each of the MT sites along a strike angle of N32°E in order to derive the most accurate regional 2-D impedances and calculate the frequency-independent twist and shear galvanic distortion parameters. Note that determining the best-fitting 2-D responses in a given coordinate system is *not* the same as rotating into that coordinate system [*Jones and Groom*, 1993; *McNeice and Jones*, 2001]. The apparent resistivities and phases were then recalculated and most of the "static shift" two-dimensional distortion effects, contained within site anisotropy, removed (see *Groom et al.* [1993] and *McNeice and Jones* [2001] for a fuller description of the methodology). The associated misfits for these decompositions indicated that the derived responses, after removal of distortion by decomposition, accurately represent all four components of the calculated ones to within a 1° error margin in phase and equivalent levels in apparent resistivity (3.5%), on average.

[33] This angle of N32°E is consistent with that obtained by *Wu et al.* [2005] for crustal and upper lithospheric mantle depths for the Wopmay orogen along Corridor 1 (Figure 1); N32°E in the upper crust N34°E for the mid-crust to N36°E for the lower crust to N43°E for the upper lithospheric mantle. However, as reported above, there is no evidence of depth-dependent variation in strike, as was observed by *Wu et al.* [2002, 2005] at sites on the eastern half of Corridors 1 and 1A with a rotation to N62°E at periods penetrating into the lower lithospheric mantle.

Table 2. Maximum Amplitudes and Directions of Reversed Real Induction Arrows for the Long-Period Sites

Site	Period of Maximum Response (s)	Amplitude of Real Induction Vector	Direction of (reversed) Real Induction Vector (degree)
001	220	0.27	33
005	220	0.23	22
009	220	0.21	38
013	220	0.31	−30
017	220	0.50	−42
021	220	0.46	−36

3.4. Two-Dimensional Modeling

[34] The distortion-corrected, regional 2-D MT responses at N32°E (TE) and N58°W (TM) were imported into Geo-

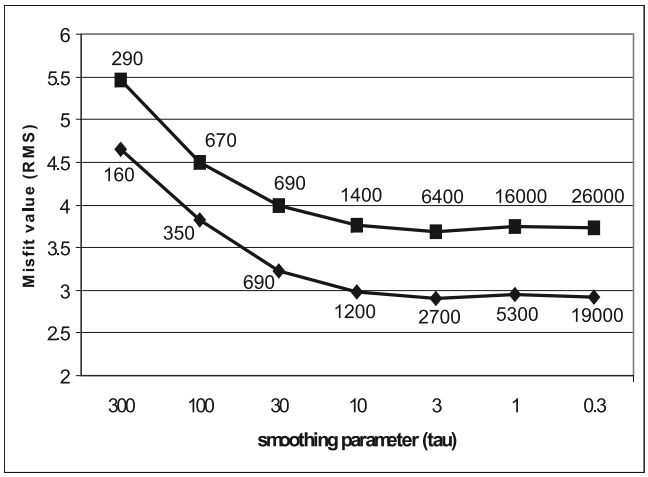

Figure 6. Graph illustrating the trade off between the RMS misfit of the model to the data and the tau value of the inversion as well as the difference in the apparent RMS value with different error floors applied to the data. The roughness of each model (sum of the lateral and vertical gradients) is given by the numeric value at each data point. The tau value chosen for the final model was 3.

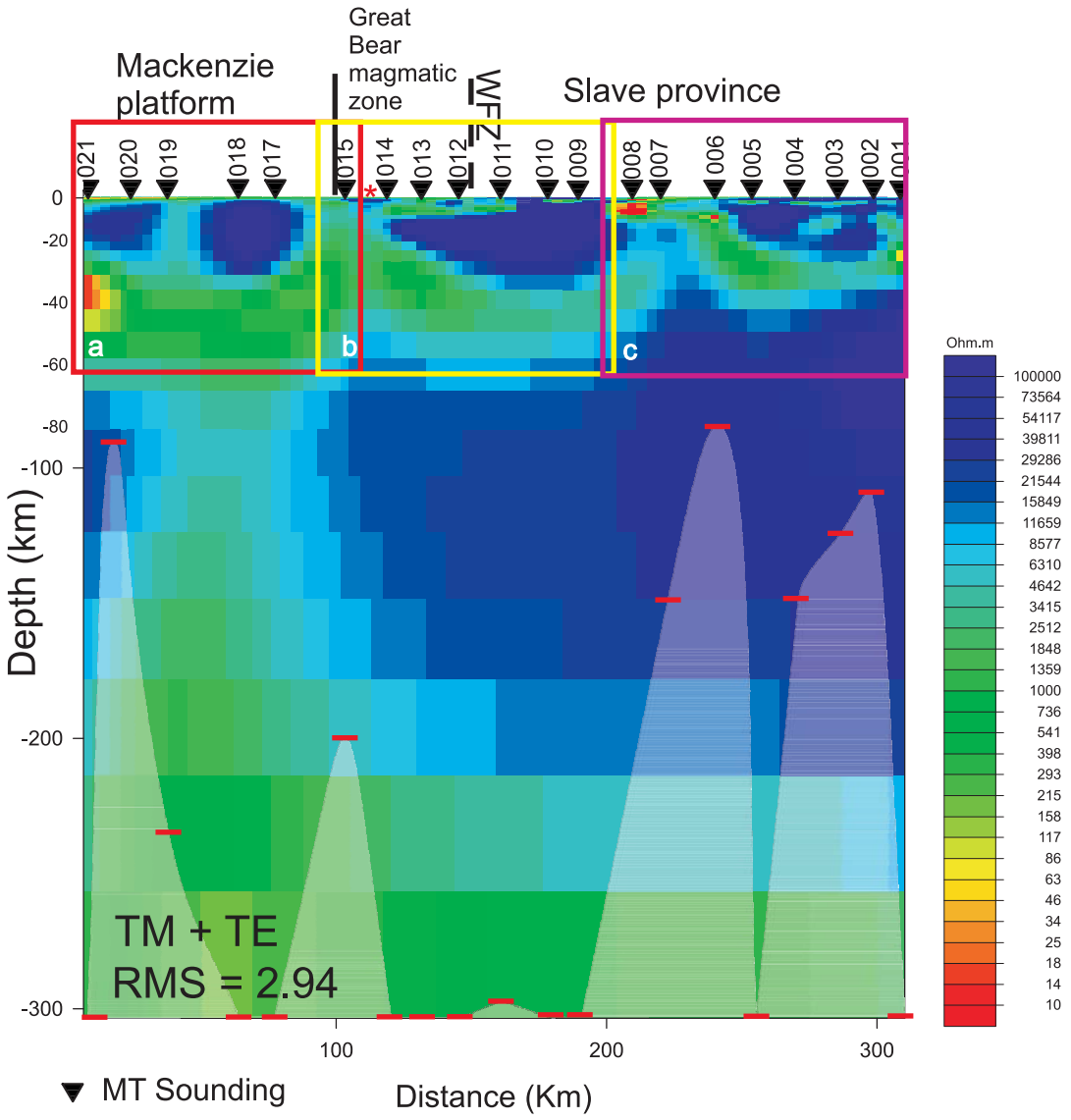

Figure 7. Final two-dimensional model produced from MT data along the Slave-to-Bear profile (see Figure 1); the red star marks the approximate location of Gameti. The warm colors represent regions of high conductivity and the colder colors represent resistive regions. The black triangles mark the site locations and the red dashes mark the calculated maximum penetration depth beneath each site (based on Schmucker's depth of penetration). The model used both the TM and TE mode components and reached an RMS value of 2.94 with a phase error floor of 1°. The squares show the sites included in the focused inversions in Figure 8.

systems's WinGLink interpretation software package that uses *Rodi and Mackie*'s [2001] latest 2-D modeling and inversion algorithm. As is common with many regularized inversion codes, this code searches iteratively for the smoothest model that best fits the data by attempting to trade off the fit to the observed data (data misfit) with the squared Laplacian (smoothing term) of the horizontal and vertical resistivity gradients. The inversion program searches for the smoothest, best-fit model with the least deviation from the starting model, which is usually a half space [*Mackie and Madden*, 1993]. This means that the models found represent the minimum structure required to fit the data with an acceptable misfit. The misfit is a standard normalized root-mean-square measured by the standard distance between the observed response and derived response normalized by variance and divided by the number of observations. One problem with this global measure of fit is that strong structure in the data, especially local structures that affect only a few sites, can be underfit by overfitting regions where there is little structure, i.e., no penalty to the smoothness measure. We address this problem below with focused inversions, i.e., inversions of local structures using fewer data from fewer sites. When inverting fewer data the responses to local-scale structures have a higher influence on the average misfit value and so are better represented in the models.

[35] Unreliable data points, with large scatter and large errors bars, were removed from the data set prior to

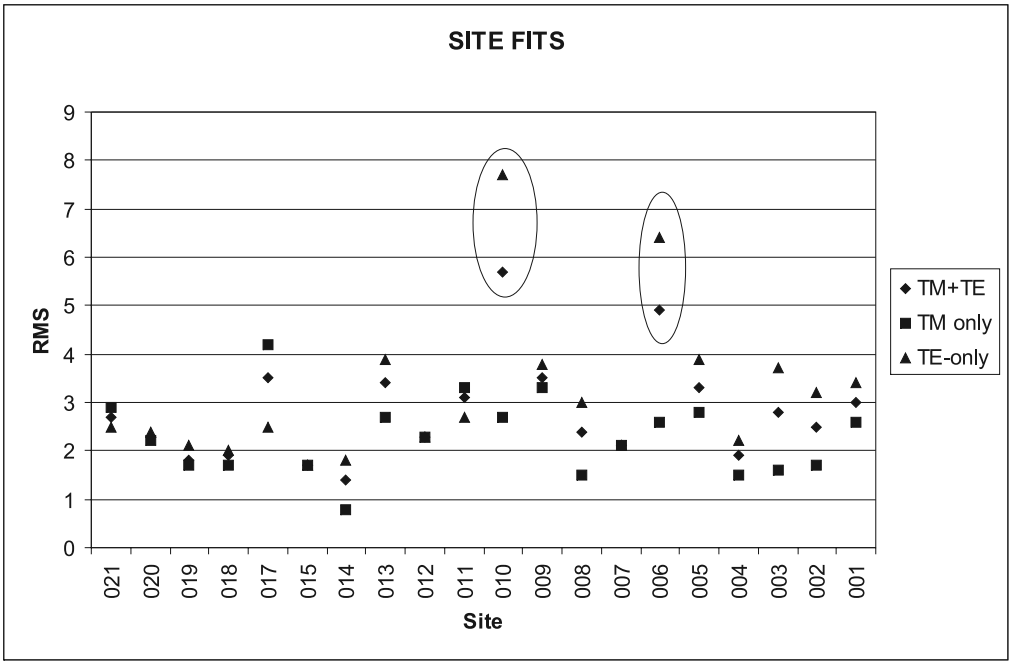

Figure 8. Individual RMS site misfits for the final two-dimensional resistivity model, shown in Figure 6, along the Slave Bear MT profile. The misfits are shown for the combined TM and TE mode data, the TM mode only data, and the TE mode only data for each site.

inversion. The inversion runs were initiated with a homogeneous half space of 100 ohm m with a mesh consisting of 50 rows and 104 columns. The phases were set with a 1° error floor, determined from the acceptable misfit values obtained in the distortion analysis. Many different models were generated using various combinations of modes and parameters in order to observe the effects of these changes on the model structure and to derive the most robust final model with an appropriate misfit value. The parameters that were varied, using combinations of TM mode, TE mode, and vertical transfer functions, included: tau (the smoothing operator), inverting for static shift, the regularization order, the smoothing parameters alpha and beta that trade-off vertical against horizontal gradient weighting, and the weighting of the regularization order.

[36] Figure 6 illustrates the trade-off between the roughness of the model, defined in terms of the tau parameter, and the fit of the data, equivalent to the so-called "L-curve" [*Hansen*, 1992; *Booker et al.*, 2004; *Farquharson and Oldenburg*, 2004], as well as the effects on the apparent misfit value when the data error floor is raised or lowered. We choose to plot misfit against tau rather than roughness itself (given by the numbers by each data point) as we have direct control on tau when undertaking the inversions. However, as can be seen in the figure, the two are almost interchangeable.

[37] The regional model chosen to most accurately represent the responses was selected by considering the features that appeared consistently between the different models, and by choosing the smoothest model with the lowest misfit. This final model, obtained after over one hundred iterations on multiple runs from inverting simultaneously both the TE- and TM mode data in the 7-decade period range 0.001–10,000 s, is shown in Figure 7 and has an overall RMS (root mean squared) misfit of 2.9 with error floors set at 1° for phase and 7% for apparent resistivity. The model was obtained with inversion parameters of τ set to 3, α and β set to 1 and the static shift option selected. The misfit of the data to the model was evaluated by plotting the RMS for each mode (TM and TE) at each site to determine whether or not the data at any particular site were fit poorly (Figure 8). The RMS for the TE mode for sites 006 and 008 are the only values above 4, and several iterations were run for the model excluding these data. The main conductivity structures in the model did not change from those shown in Figure 7, but the overall RMS reduced to 2.7.

[38] In order to refine the conductivity structure at crustal depths, additional models where derived using higher frequencies for selected sites along the MT profile (Figure 9). The modeling parameters and techniques applied were similar to those used to produce the whole profile model described above. These inversions, which focused on fitting fewer data from fewer sites using a smaller model with a finer mesh, resulted in an RMS value of 2.6 for the western end of the profile, the region beneath the Phanerozoic platform sedimentary rocks (Figure 9A), an RMS of 2.4 for the region crossing the Wopmay fault zone (Figure 9B), and an RMS of 2.5 for the exposed Slave craton, the eastern end of the profile (Figure 9C). The three focused models reveal much more detail in the conductivity structure at crustal depths beneath the profile. It should be noted that these models illustrate the minimum structure required to fit the data, and that definition of the shallow upper crustal structures is limited by the 20 km station spacing.

4. Interpretations and Discussion

4.1. Strike Direction

[39] Generally, the region exhibits low dimensionality, and is one-dimensional or weakly two-dimensional at most

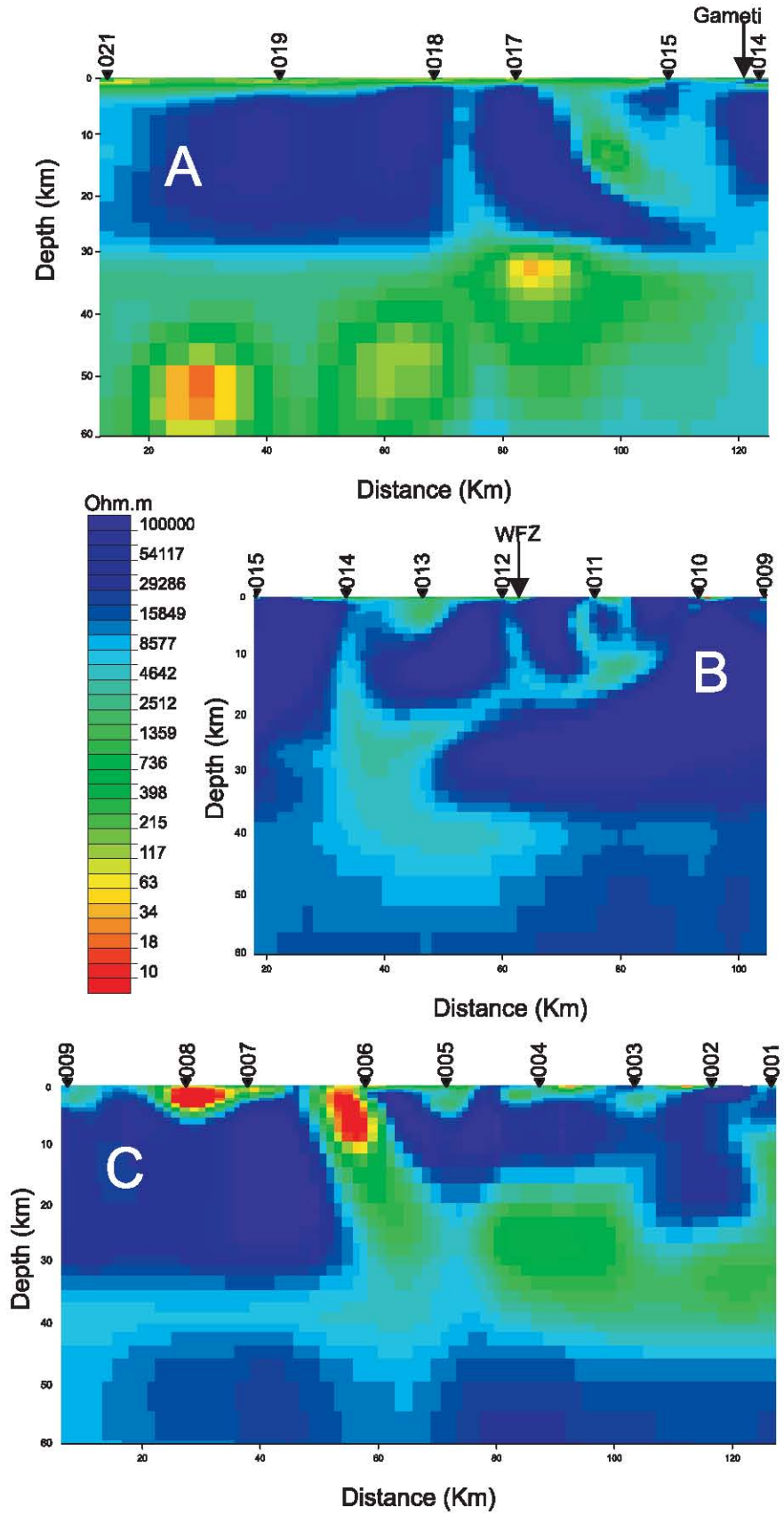

Figure 9. Crustal-scale models produced from three sections along the main Slave-to-Bear profile: (A) a two-dimensional model of the western-most six sites showing the crustal structure in the Bear Province, (B) a model across the Wopmay fault zone, and (C) a model of the eastern-most nine sites illustrating the crustal structure in the Slave Province.

sites. The geoelectric strike direction is reasonably uniform in both horizontal direction and with period (proxy for depth) (Figure 5), with a best-fit average strike of N32°E. This value is consistent with that observed by *Wu et al.* [2005] for the crust and upper lithospheric mantle at sites on the eastern part of Corridor 1 that crosses the Hottah terrane and Great Bear magmatic zone, but differs significantly from their strike for the lower lithosphere of their region of N62°E. For the Great Slave Lake shear zone (Figure 1, GSLsz), a lithospheric geoelectric strike of ∼N65°E [*Wu et al.*, 2002; *Eaton et al.*, 2004] was observed, which is 20° oblique to the absolute plate motion (APM) direction of the region of N135°W (determined using model HS3-NUVEL-1A of *Gripp and Gordon* [2002] with K. Okino's calculator at ofgs.ori.u-tokyo.ac.jp/∼okino/platecalc_new.html).

[40] This lack of evidence of a strike with either a GSLsz orientation of ∼N65°E or with an APM direction of ∼N45°E in our study region we take as evidence that the crust and lithospheric mantle responded coherently during Paleoproterozoic deformation, and that the fabric introduced has not been reset by subsequent processes, including present day plate motions.

[41] We note that our geoelectric strike direction of N32°E is oblique to the preliminary SKS results for POLARIS seismic sites GALN and CTLN (Figure 2) reported in *Snyder and Bruneton* [2007]. Those authors reported parameters from both best-fitting single layer and two layer models to the data, with GALN giving a single layer direction of N19°E and two-layers of N55°E on top of N18°E and CTLN giving N50°E for a single layer and N85°E on top of N0°E for two-layers. None of these directions are within experimental error of N32°E, thus we can exclude anisotropy caused by preferential alignment of olivine as an explanation of the observed geoelectric strike.

4.2. Crust-Mantle Depth

[42] Figure 10 illustrates various large-scale features that are consistent among the various models generated. The deep structure revealed includes the crust-mantle transition and the depth extent of cratonic roots. The yellow line most likely represents the electric crust-mantle boundary, separating the resistive cratonic crustal granitoids above from the more conductive underlying lithospheric mantle. Note that typically the crust-mantle transition cannot be imaged by magnetotellurics because of the shielding effect of lower crustal conducting layers. Where the lower crust is resistive however, such as on the Slave craton [*Jones and Ferguson*, 2001], the Rae Craton [*Jones et al.*, 2002] and the East Indian Craton [*Bhattacharya and Shalivahan*, 2002], this boundary can be defined electrically. The model shows that a crustal thickness of 32–35 km remains fairly constant beneath both the Slave craton and within the Wopmay orogen beneath the Great Bear magmatic zone. This is consistent with interpretations of the LITHOPROBE refraction/wide-angle reflection survey across these terranes further south along Corridor 1 [*Fernández-Viejo and Clowes*, 2003].

4.3. Wopmay Mantle

[43] The dashed white lines in Figure 10 illustrate major lateral changes of electrical resistivity within the upper mantle. The base of the lithosphere appears to begin at ∼210 km at the eastern most part of the profile and shallows to ∼150 km beneath the western edge of the Slave craton. This value of 210 km is consistent with that observed in the center of the Slave craton, both geophysically and petrologically (see above). At depths of ∼100 km there is a distinct decrease in the overall apparent resistivity (∼2500 ohm m) within the lithosphere directly beneath the surface-mapped boundary between the Great Bear magmatic zone and the Phanerozoic platform compared to the neighboring resistive mantle (>50,000 ohm m). This may mark the western edge of the resistive cratonic root beneath the Slave Province. West of the Great Bear magmatic zone the lithosphere again becomes more resistive, and appears to thicken toward the western edge of the profile. Although there is no data coverage west of our profile, this apparent thickening in the western part would not be observed if the lithosphere significantly thinned further to the west.

[44] *Wu et al.* [2005] observed a region of enhanced conductivity (<10 ohm m) at similar depths beneath the Hottah terrane in the Lithoprobe profile near the southern margin of the Slave craton. They interpret this region of high conductivity to be carbon or sulfides that were introduced into the mantle as sediments in a subduction setting during the collision and accretion of the Hottah terrane to the western margin of the Slave craton. There is a difference of nearly an order of magnitude in the conductivity values of this mantle conductor between *Wu et al.*'s [2005] results and those observed along our northern profile, indicating that there is significant variation in the along-strike mantle conductivity structure. This would suggest, as seen within the Trans-Hudson orogen [*Jones et al.*, 1997, 2005], that the presence of interconnected carbon and/or sulfides is not continuous along the orogen, and carbon is not taken to explain the mildly enhanced conductivity along our central profile.

[45] Laboratory studies indicate that the electrical resistivity of olivine at the expected pressure-temperature conditions for these depths should be >100,000 ohm m [*Constable and Duba*, 1990; *Constable*, 2006]. The two pyroxenes bracket olivine in their temperature-resistivity relationships [*Xu et al.*, 2000], and mixing relations of the two pyroxenes and olivine to yield mantle compositions yield values close to olivine on its own [*Ledo and Jones*, 2005].

[46] The variations shown in this profile range from >50,000 ohm m beneath the cratons, consistent with laboratory studies on dry mantle minerals, to ∼2500 ohm m between the cratons, a change of just over an order of magnitude. Enhanced conductivity in the lithospheric mantle has been attributed to fluids or melt [*Glover et al.*, 2000], grain boundary carbon films [*Duba and Shankland*, 1982] or carbon on fractures [*Mareschal et al.*, 1995; *Roberts et al.*, 1999], interconnected sulfides [*Ducea and Park*, 2000], hydrous minerals [*Boerner et al.*, 1999], and hydrogen diffusion [*Karato*, 1990; *Hirth et al.*, 2000], but small amounts of these typically invoke changes in conductivity of several orders of magnitude [*Jones*, 1999; *Jones and Ferguson*, 2001].

[47] None of these explanations is without serious objection for the lithospheric mantle beneath the Wopmay orogen. On the basis of critical dihedral angle arguments,

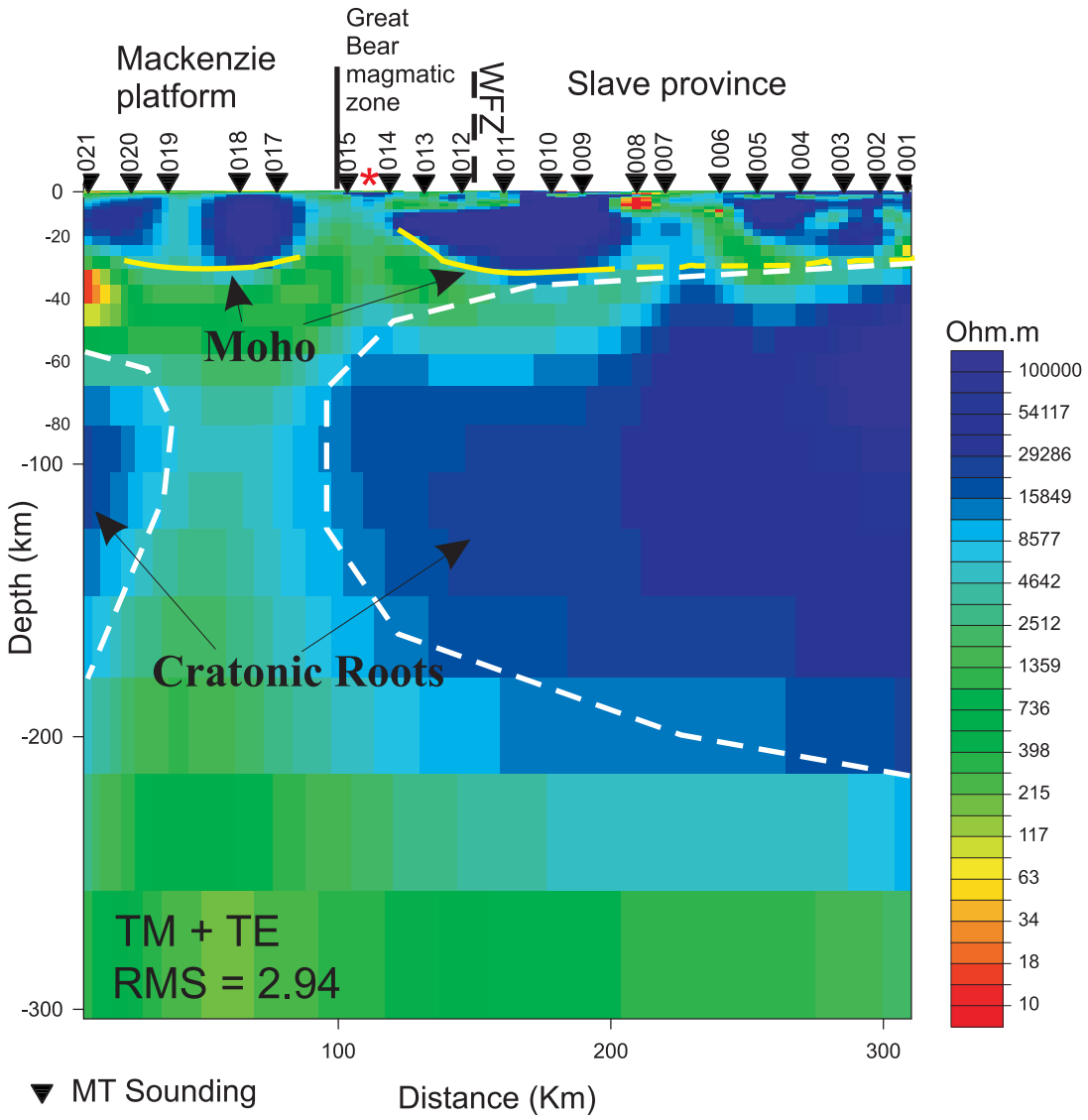

Figure 10. Interpretations of the conductivity structure revealed in the two-dimensional model shown in Figure 6. The red star marks the approximate location of Gameti. The yellow line marks the crust mantle boundary and the white dashed lines indicate the cratonic roots beneath both the Slave and the Bear provinces.

water-based fluids will not be connected until the pressure is in excess of 2 GPa, i.e., about 60 km depth [*Mibe et al.*, 1998], whereas we observe enhanced conductivity directly below the Moho to about 80 km depth. Also, fluids will not stay resident in the lithosphere since Precambrian times. Partial melts in an elevated lithosphere-asthenosphere boundary can be excluded as there is no other supporting evidence for this, including the only heat flow value on the Wopmay orogen at the Muskox intrusion exhibiting only a mildly increased value of 54 mW m^{-2} [*Beck and Sass*, 1966] compared to the Slave cratonic average of 46 mW m^{-2} [*Mareschal et al.*, 2004]. (Even though this difference is small, it is consistent with petrological analyses of Slave craton mantle xenoliths that show the Slave craton to be cooler than other Archean cratons [*Kopylova et al.*, 1999].) Carbon will be conductive in the upper lithosphere, but below the graphite-diamond stability field (~150 km depth) it will be in the form of highly resistive diamond. Sulfides are possible; *Alard et al.* [2000] show evidence that sulfide is mobile in the lithosphere and can concentrate upward to crystallize and concentrate at shallow depths. Enclosed sulfides will not enhance conductivity, but interstitial sulfides precipitated from metasomatic fluids may form a connected electrical pathway. There is no supporting evidence for this conjecture, however *Pearson et al.* [1999] note that the mantle of the Slave craton is far less metasomatized than that of the Kaapvaal craton, for which the sulfide data exist. The presence of hydrous minerals, such as phlogopite [*Boerner et al.*, 1999] is highly unlikely to enhance conductivity, as they are not interconnected when in xenolith samples. This is also excluded on the basis of lack of evidence of metasomatism, as is hydrogen diffusion [*Karato*, 1990] on the same grounds. Ironically, the most metasomatized lithosphere in the whole of Canada exists beneath the

Rae-Hearne contact in the Western Churchill Province, and there the lithospheric mantle is highly resistive [*Jones et al.*, 2002].

[48] As an alternative and viable explanation, recently *Ten Grotenhuis et al.* [2004] showed, for micrometer-sized samples, that there is an inverse relationship between the electrical conductivity of mantle olivine and its grain size, where a significant increase in grain size is extrapolated to lower the conductivity by up to 2 orders of magnitude. They suggest that a decrease in grain size to a minimum of 1 cm has no effect on the electrical conductivity. Where there is a stable mantle grain size of >1 cm, as predicted for stable mantle olivine at these depths based on mantle xenolith observations [see references in *Hirth and Kohlstedt*, 2003], there would have to be a reduction in grain size to 100 micrometers to obtain the values observed beneath the Wopmay orogen, indicating the presence of a mantle shear zone at depths of 70–80 km in this region.

[49] The presence of an east-dipping mantle shear zone is supported by seismic reflection data that imaged reflectivity to about 82 km in the mantle in the vicinity of the Hottah-Slave transition. *Cook et al.* [1999] suggested that was evidence for polarity reversal of the subduction zone created by the accreting Hottah terrane, although the 2-D MT model (Figure 7) does not indicate reduce resistivity dipping beneath the Slave craton. Evidence for a mantle shear zone at this location indicates a modification of the mantle to accommodate subduction during the collision and accretion of the Hottah terrane to the western margin of the Slave craton.

4.4. Slave Upper Mantle

[50] Similar to tectonic models of the Snowbird Tectonic Zone [*Jones et al.*, 2002], the deep resistivity model shows that the western edge of the resistive upper mantle root beneath the Slave craton is not located directly beneath the Wopmay fault zone, but lies further to the west beneath the Great Bear magmatic zone (Figure 10). This suggests that the resistive Slave upper mantle has been underthrust westward beneath the Wopmay crust by more than 50 km, indicating decoupling between the crust and the upper mantle at the Moho. These results are consistent with the cross-section illustrated by *Cook et al.* [1999], but the offset is shown to be approximately 100 km (Figure 3). This suggests again along strike variations in the mantle structure beneath this region.

[51] There is no indication of an anomalous low-resistivity zone (<100 ohm m) in the mantle beneath any part of this profile, suggesting that the Central Slave Mantle Conductor is not located beneath the region and that its western margin lies further to the east. The presence of a mantle conductor beneath the Slave craton has been linked to the presence of diamondiferous kimberlites [*Jones and Craven*, 2004]. The absence of a mantle conductor in the study area could have implications for the diamond potential of the area; however, no upper mantle conductor has been detected beneath the diamond producing Kaapvaal craton in South Africa. Mapping the extent of the Central Slave mantle conductor may have important implications on diamond exploration in northern Canada and may help to further compare the Slave and other Archean cratons.

4.5. Crust and Upper Mantle Structure of the Wopmay Orogen

[52] In the western third of the profile (Figure 9A), west of the Wopmay fault zone, there is a moderately conductive (~100 ohm m) thin layer near the surface, beginning near site 015 and thickening slightly to depths of 1–2 km beneath the western-most site. This most likely represents the Phanerozoic sedimentary platform that covers much of the region (Figures 1 and 2).

[53] Beneath this layer the conductivity of the crust of the Bear Province is relatively featureless with resistivities >10,000 ohm m to depths of 30–32 km. *Wu et al.* [2005] show a major conductor at mid-crustal depths at the boundary between the Hottah terrane and the neighboring Fort Simpson terrane. The lack of a conductor in these focused models indicates that either there are significant changes in the conductivity structure from south to north or, more likely, that the northern MT profile does not extend beyond the Paleozoic rocks of the Wopmay orogen into the Fort Simpson terrane.

[54] The upper mantle beneath this region is shown to be moderately resistive (100–1000 ohm m), at depths of 35–60 km, compared to that further to the east (Figure 11), but not as conductive as the Central Slave mantle conductor (10–30 ohm m), nor as conductive as the feature found in the Hottah mantle beneath Corridor 1 [*Wu et al.*, 2005], also around 10–30 ohm m. This is an indication that beneath the Hottah terrane the origin of the mantle material, or processes involved in its formation and evolution as preserved now, are different to those that generated the mantle beneath the east-central part of the Slave Province.

[55] In the regional two-dimensional model of the entire data set (Figure 7), the area beneath the Great Bear magmatic zone of the Wopmay orogen appears to have a general increased conductivity in the mid-to-lower crust. However the focused inversion of this region shows significantly more structure (Figure 9B) because of the requirement in these focused inversions to fit local-scale structures. In general, at crustal depths in the vicinity of the Wopmay fault zone there appears to be a change from very uniform resistive (>10,000 ohm m) material to the east to a less resistive (~2000 ohm m), structurally complex region to the west. This is interpreted to be the boundary between the Slave crust and the rocks of the Wopmay orogen (Figure 11).

[56] Directly beneath the surficial trace of the Wopmay fault zone there is a near-vertical, slightly less resistive anomaly of ~5000 ohm m within an extremely resistive upper crust at ~100,000 ohm m (Figure 11). Fluids and/or mineralization are often used to interpret zones of enhanced conductivity within fault planes [*Jones et al.*, 1992, 1997; *Wannamaker et al.*, 2002; *Ritter et al.*, 2005]. Fluids are an unlikely source for the feature here because it is not probable for fluids to remain trapped in a stable area for long periods of time. Additionally, the presence of interconnected saline fluids, even a small amount, typically increases the conductivity values by several orders of magnitude [*Nesbitt*, 1993; *Partzsch et al.*,

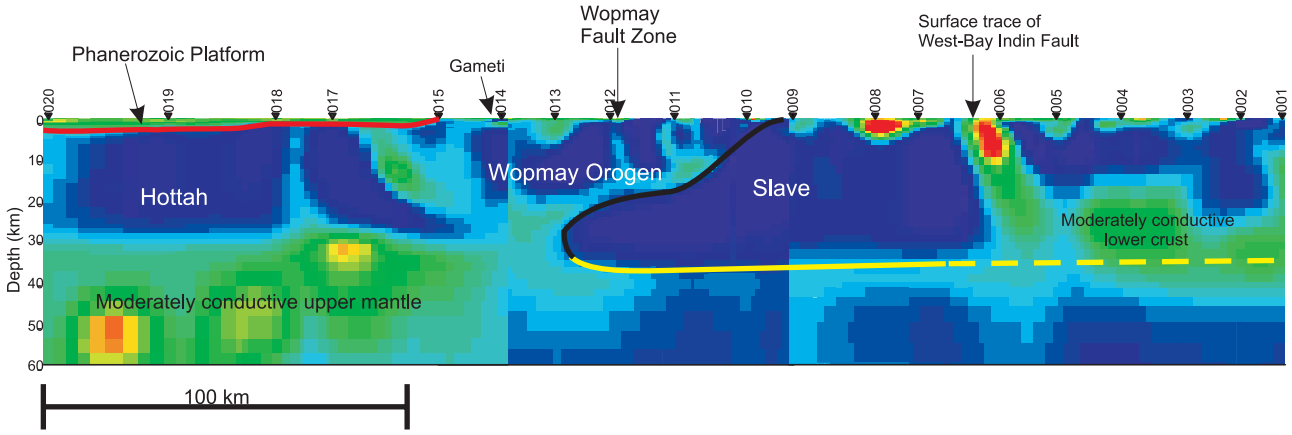

Figure 11. Interpretations of the conductivity structure revealed in the three separate focused inversions shown in Figure 9. The yellow line marks the crust mantle boundary, the red line indicates the depth extent of the Phanerozoic platform, and the black line illustrates the boundary between rocks of the Slave Province to the east and those of the Wopmay orogen to the west.

2000] greater than the increase seen under the Wopmay fault zone. The less resistive structure beneath the fault zone is still within the range for typical crustal materials, and most probably represents a structural alignment of grains or metallic mineralization along the fault plane. However, the presence of interconnected sulfides or graphite would typically increase the conductivity value by several orders of magnitude. Structural alignment and reduced grains size in the area is confirmed by bedrock mapping, as mylonites are commonly encountered along this zone [*Jackson*, 2006].

[57] The Wopmay fault zone has been interpreted to be a major crustal-scale feature and has been suggested to represent the suture between the Archean Slave craton and the cryptic Aphebian Hottah microcontinent [*Bowring and Podosek*, 1989], where the fault extends to the crust-mantle boundary [*Bleeker*, 2003]. In contrast to these concepts, the feature illustrated in the MT model only extends to a depth of 20 km (Figure 11), inferring that the Wopmay fault zone does not penetrate through the entire crust. This supports results from the seismic reflection profile across the southern margin of the Slave craton, which indicates that if faults associated with the Wopmay fault zone are present at the survey location, either they do not penetrate to depths greater than 15 km, or they flatten out listrically into west dipping layers [*Cook et al.*, 1999]. These westward-dipping layers mark the upper boundary of the intra-crustal cratonic wedge of the Slave craton. Unfortunately, the profile orientation and proximity of the Great Slave Lake shear zone of the Lithoprobe MT data in the vicinity of the southern extent of the Wopmay fault zone prevents an accurate image of its conductivity structure, and along strike comparisons cannot be assessed.

4.6. Crustal Structure of the Slave Craton

[58] The focused inversion of the data from within the Slave Province, the eastern-most sites along the profile, reveals two significant conductivity anomalies: the first is a shallow structure beneath site 008, and the second is an eastward-dipping structure extending from the surface just west of site 006 (Figure 9C). The shallow conductive body ($\sim$10 ohm m) beneath site 008 occurs at a depth of <2 km and appears to lie on the mapped boundary between a sequence of low-grade metasediments and felsic-volcanic rocks (Figure 2). Although sedimentary rocks are often highly conductive compared to granites and show up well in MT models, the metasedimentary unit here is widespread, whereas this conductive anomaly appears to be localized in extent and is not seen on adjacent sites. Along with a slight aeromagnetic anomaly [*Dods et al.*, 1989], sulfide-bearing gossans have been observed along this geological contact [*Jackson*, 2006] and a localized body of interconnected sulfides is the most likely cause for the conductivity anomaly.

[59] The second conductivity anomaly is eastward-dipping and extends from the surface to at least 30 km depth within the crust (Figure 9C), with most conductive material above 10 km. The location of the surface expression of the eastern edge of this conductive zone, located between sites 006 and 007, spatially correlates closely with that of the West-Bay-Indin fault zone (Figures 2 and 11). The focused 2-D model for this feature is similar to that produced from MT data across the Yellowknife River fault zone [*Jones and Garcia*, 2006] and is consistent with the interpretation that these are large, crustal-scale faults. The weakly enhanced conductivity in the Yellowknife River fault zone was attributed to sulfide mineralization within the fault plane on the basis of laboratory physical property studies on rocks from the area [*Katsube et al.*, 2006]. Similar mineralization processes may responsible for the enhanced conductivity in the West-Bay-Indin fault zone and/or parallel neighboring fault systems.

[60] Additionally, in comparison to the rest of the profile and to other MT models of the Slave craton [*Jones and Ferguson*, 2001; *Jones et al.*, 2001, 2003], the focused model beneath the western Slave (Figure 11) indicates a moderately resistive lower crust ($\sim$500 ohm m) beneath a very resistive mid-crust (>10,000 ohm m). This elevated conductivity, like that beneath the Wopmay fault zone, is typical for resistivity values of crustal material, but creates a

shadowing effect whereby the crust-mantle boundary cannot be well defined. The change in conductivity with depth in the crust may represent a mafic lower crust beneath the crystalline plutonic rocks within the Slave craton.

5. Conclusions

[61] A magnetotelluric experiment was performed across the boundary between the western Slave craton and the Bear Province in the Northwest Territories, Canada, and the data provide information about the resistivity structure of the crust and lithospheric mantle beneath the profile. Strike analysis and distortion decomposition on these data indicated that most of the data along the profile are two-dimensional and fit a regional geoelectric strike angle of N32°E. This angle is consistent with that obtained further to the south along the Lithoprobe profile at crustal depths and is likely to be controlled by transcurrent faults observed throughout the region. The two-dimensional models generated, with responses estimated in that coordinate system, show both regional-scale features correlating with major tectonic events and small-scale features that can be attributed to local geologic structure.

[62] The two-dimensional model of the MT data shows the crust-mantle boundary to exist at approximately 32–35 km beneath the profile and indicates conductivity variations in the lithospheric mantle. Resistive zones are seen beneath the Slave craton and beneath the Hottah terrane, and these zones are separated by a less resistive region. There are few plausible candidates to explain enhanced conductivity in the lithospheric mantle of Precambrian regions, and none without serious objection. Although somewhat speculative, the increase in conductivity at 60–80 km depths in the mantle beneath the Great Bear magmatic zone we conjecture to represent a decrease in the grain size of olivine in the Wopmay mantle compared to its neighboring cratonic roots. The presence of a mantle shear zone related to ancient subduction would have an important influence of the deformation history and geodynamic modeling of the region.

[63] At shallower depths, the crustal-scale two-dimensional focused models reveal more structure than the whole profile model. In general, there appears to be a change, from very uniform resistive material to the east to a less resistive, structurally complex region to the west. This is interpreted to represent the boundary between the Slave crust and the rocks of the Wopmay orogen and suggests that the eastern extent of the crustal Slave cratonic root crosses the Wopmay fault zone. The focused model indicates that the Wopmay fault zone does not extend into the deep lower crust, but may develop into westward dipping layers that mark the top of an intracrustal cratonic wedge. Further to the east, an eastward-dipping conductor is interpreted as sulfide mineralization within the West-Bay-Indin fault zone that does appear to extend to the base of the crust through the Slave craton. Additionally, a shallow conductive body beneath site 008 occurs at a depth of <2 km, that lies on the mapped boundary between a sequence of low-grade metasediments and felsic-volcanic rocks, and is interpreted to represent a region of localized interconnected sulfides.

[64] **Acknowledgments.** Financial support for this project came from the Department of Indian Affairs and Northern Development (DIAND) Geology Division. The fieldwork was completed with the help from Carolyn Relf and colleagues at the NWT Geoscience Centre (Yellowknife, NWT), the Geological Survey of Canada, as well as support from all the crew at the Koropchuk Lake field camp. Additional help came from L. Ootes for generating the detailed location map of the survey area and for providing insightful, editorial comments and suggestions. This paper was improved through positive comments received from the two external reviewers. NTGO contribution 0037.

References

Alard, O., W. L. Griffin, J. P. Lorand, and S. E. O'Reilly (2000), Non-chondritic distribution of the highly siderophile elements in mantle sulfides, *Nature*, *407*, 891–894.

Anderson, F., D. E. Boerner, K. Harding, A. G. Jones, R. D. Kurtz, J. Parmelee, and D. Trigg (1988), LIMS: Long period intelligent magnetotelluric system, paper presented at the 9th Workshop on EM Induction Sochi, USSR, 24–31 October.

Beck, A. E., and J. H. Sass (1966), A preliminary value of heat flow at the Muskox intrusion, near Coppermine N.W.T., Canada, *Earth Planet. Sci. Lett.*, *1*, 123–129.

Bennett, V., V. A. Jackson, T. Rivers, C. Relf, P. Horan, and M. Tubrett (2005), Geology and U-Pb geochronology of the Neoarchean Snare River terrane: Tracking evolving tectonic regimes and crustal growth mechanisms, *Can. J. Earth Sci.*, *42*, 895–934.

Bhattacharya, B. B., and Shalivahan (2002), The electric Moho underneath Eastern Indian Craton, *Geophys. Res. Lett.*, *29*(10), 1376, doi:10.1029/2001GL014062.

Bleeker, W. (2002), Archean tectonics—A review, with illustrations from the Slave craton, *Geol. Soc. Spec. Publ.*, *199*, 151–181.

Bleeker, W. (2003), The late Archean record: A puzzle in ca. 35 pieces, *Lithos*, *71*, 99–134.

Bleeker, W., J. W. F. Ketchum, V. A. Jackson, and M. E. Villeneuve (1999a), The Central Slave basement complex. part I: Its structural topology and autochthonous cover, *Can. J. Earth Sci.*, *36*, 1083–1109.

Bleeker, W., J. W. F. Ketchum, and W. J. Davis (1999b), The Central Slave basement complex. part II: Age and tectonic significance of high-strain zones along the basement-cover contact, *Can. J. Earth Sci.*, *36*, 1111–1130.

Boerner, D. E., R. D. Kurtz, and J. A. Craven (1996), Electrical conductivity and Paleoproterozoic foredeeps, *J. Geophys. Res.*, *101*, 13775–13789.

Boerner, D. E., R. D. Kurtz, J. A. Craven, G. M. Ross, F. W. Jones, and W. J. Davis (1999), Electrical conductivity in the Precambrian lithosphere of western Canada, *Science*, *283*, 668–670.

Booker, J. R., A. Favetto, and M. C. Pomposiello (2004), Low electrical resistivity associated with plunging of the Nazca flat slab beneath Argentina, *Nature*, *429*, 399–403.

Bowring, S. A. (1985), U-Pb zircon geochronology of early Proterozoic Wopmay orogen, NWT, Canada: An example of rapid crustal evolution, unpublished Ph.D. thesis, Univ. of Kansas, Kans.

Bowring, S. A., and J. P. Grotzinger (1992), Implications of new chronostratigraphy for tectonic evolution of Wopmay orogen, northwest Canadian Shield, *Am. J. Sci.*, *292*, 1–20.

Bowring, S. A., and F. A. Podosek (1989), Nd isotopic evidence from Wopmay orogen for 2.0–2.4 Ga crust in western North America, *Earth Planet. Sci. Lett.*, *94*, 217–230.

Cagniard, L. (1953), Basic theory of the magnetotelluric method of geophysical prospecting, *Geophysics*, *18*, 605–635.

Camfield, P. A., J. C. Gupta, A. G. Jones, R. D. Kurtz, D. H. Krentz, J. A. Ostrowski, and J. A. Craven (1989), Electromagnetic sounding and crustal electrical conductivity structure in the region of the Wopmay orogen, Northwest Territories, Canada, *Can. J. Earth Sci.*, *26*, 2385–2395.

Chave, A. D., and A. G. Jones (1997), Electric and magnetic field distortion decomposition of BC87 data, *J. Geomagn. Geoelectr.*, *49*, 767–789.

Clowes, R. M., P. T. C. Hammer, G. Fernández-Viejo, and J. K. Welford (2005), Lithospheric structure in northwestern Canada from Lithoprobe seismic refraction and related studies: A synthesis, *Can. J. Earth Sci.*, *42*, 1277–1293.

Constable, S. C. (2006), SEO3: A new model of olivine electrical conductivity, *Geophys. J. Int.*, *166*, 435–437.

Constable, S., and A. Duba (1990), Electrical conductivity of olivine, a dunite, and the mantle, *J. Geophys. Res.*, *95*, 6967–6978.

Cook, F. A., and P. Erdmer (2005), An 1800 km cross section of the lithosphere through the northwestern North American plate: Lessons from 4.0 billion years of Earth's history, *Can. J. Earth Sci.*, *42*, 1295–1311.

Cook, F. A., A. J. van der Velden, K. W. Hall, and B. J. Roberts (1998), Tectonic delamination and subcrustal imbrication of the Precambrian lithosphere in northwestern Canada mapped by Lithoprobe, *Geology*, *26*, 839–842.

Cook, F. A., A. J. van der Velden, and K. W. Hall (1999), Frozen subduction in Canada's Northwest Territories: Lithoprobe deep lithospheric reflection profiling of the western Canadian Shield, *Tectonics*, *18*, 1–24.

Davis, W. J., and E. Hegner (1992), Neodymium isotopic evidence for the tectonic assembly of late Archean crust in the Slave Province, northwest Canada, *Contrib. Mineral. Petrol.*, *111*, 493–504.

Davis, W. J., and W. Bleeker (1999), Timing of plutonism, deformation, and metamorphism in the Yellowknife Domain, Slave Province, Canada, *Can. J. Earth Sci.*, *36*, 1169–1187.

Davis, W. J., C. Gariepy, and O. van Breemen (1996), Pb isotopic composition of late Archean granites and the extent of recycling early Archean crust in the Slave Province, northwest Canada, *Chem. Geol.*, *130*, 255–269.

Davis, W. J., A. G. Jones, W. Bleeker, and H. Grutter (2003), Lithosphere development in the Slave craton: A linked crustal and mantle perspective, *Lithos*, *71*, 575–589.

d'Erceville, I., and G. Kunetz (1962), The effect of a fault on the Earth's natural electromagnetic field, *Geophysics*, *27*, 651–665.

Dods, S. D., D. J. Teskey, and P. J. Hood (1989), Magnetic anomaly map of Canada, *Map 11*, scale 1:10,000,000, Geol. Surv. of Can., Can. Geophys. Atlas.

Duba, A. L., and T. J. Shankland (1982), Free carbon and electrical conductivity in the Earth's mantle, *Geophys. Res. Lett.*, *9*, 1271–1274.

Duba, A., S. Heikamp, W. Meurer, G. Nover, and G. Will (1994), Evidence from borehole samples for the role of accessory minerals in lower crustal conductivity, *Nature*, *367*, 59–61.

Ducea, M. N., and S. K. Park (2000), Enhanced mantle conductivity from sulfide minerals, southern Sierra Nevada, California, *Geophys. Res. Lett.*, *27*, 2405–2408.

Eaton, D. W., A. G. Jones, and I. J. Ferguson (2004), Lithospheric anisotropy structure inferred from collocated teleseismic and magnetotelluric observations: Great Slave Lake shear zone, northern Canada, *Geophys. Res. Lett.*, *31*, L19614, doi:10.1029/2004GL020939.

Evans, S., A. G. Jones, J. Spratt, and J. Katsube (2005), Central Baffin electromagnetic experiment (CBEX) maps the NACP in the Canadian arctic, *Phys. Earth Planet. Inter.*, *150*, 107–122.

Farquharson, C. G., and D. W. Oldenburg (2004), A comparison of automatic techniques for estimating the regularization parameter in non-linear inverse problems, *Geophys. J. Int.*, *156*, 411–425.

Fernández-Viejo, G., and R. M. Clowes (2003), Lithospheric structure beneath the Archaean Slave Province and Proterozoic Wopmay orogen, northwestern Canada, from a Lithoprobe refraction/wide-angle reflection survey, *Geophys. J. Int.*, *153*, 1–19.

Fraser, J. A. (1967), Geology Hardisty Lake, West Half, District of Mackenzie, *Map 1224A*, "A" series map, scale 1:253,440, Geol. Surv. of Can.

Glover, P. W. J., J. Pous, P. Queralt, J.-A. Munoz, M. Liesa, and M. J. Hole (2000), Integrated two-dimensional lithospheric conductivity modeling in the Pyrenees using field-scale and laboratory measurements, *Earth Planet. Sci. Lett.*, *178*, 59–72.

Gripp, A. E., and R. G. Gordon (2002), Young tracks of hotspots and current plate velocities, *Geophys. J. Int.*, *150*, 321–361.

Groom, R. W., and R. C. Bailey (1989), Decomposition of magnetotelluric impedance tensors in the presence of local three-dimensional galvanic distortion, *J. Geophys. Res.*, *94*, 1913–1925.

Groom, R. W., R. D. Kurtz, A. G. Jones, and D. E. Boerner (1993), A quantitative methodology for determining the dimensionality of conductive structure from magnetotelluric data, *Geophys. J. Int.*, *115*, 1095–1118.

Haak, V., and R. Hutton (1986), Electrical resistivity in continental lower crust, in *Nature of Lower Continental Crust*, edited by J. B. Dawson et al., *Geol. Soc. London Spec. Publ.*, *24*, 35–49.

Hanmer, S. (1988), Great Slave Lake shear zone, Canadian Shield: Reconstructed vertical profile of a crustal-scale fault zone, *Tectonophysics*, *149*, 245–264.

Hansen, P. C. (1992), Analysis of discrete ill-posed problems by means of the L-curve, *SIAM Rev.*, *34*, 561–580.

Hildebrand, R. S., and S. A. Bowring (1987), Tectono-magmatic evolution of the 1.9-Ga Great Bear magmatic zone, Wopmay orogen, Northwestern Canada, *J. Volcanol. Geotherm. Res.*, *32*, 99–118.

Hildebrand, R. S., S. A. Bowring, and T. Housh (1990), The medial zone of Wopmay orogen, District of Mackenzie, *Geol. Surv. of Can. Pap. 90-1C*, pp. 167–176.

Hirth, G., and D. Kohlstedt (2003), Rheology of the upper mantle and the mantle wedge: A view from experimentalists, inside the subduction factory, *Geophys. Monogr.*, *138*, 83–105.

Hirth, G., R. L. Evans, and A. D. Chave (2000), Comparison of continental and oceanic mantle electrical conductivity: Is the Archean lithosphere dry?, *Geochem. Geophys. Geosyst.*, *1*(12), 1030, doi:10.1029/2000GC000048.

Hoffman, P., and L. Hall (1993), Geology, Slave craton and environs, District of Mackenzie, Northwest Territories, *Geol. Surv. of Can. Open File Rep. 2559*, scale 1:1,000,000.

Hoffman, P. F., and S. A. Bowring (1984), Short-lived 1.9 Ga continental margin and its destruction, Wopmay orogen, Northwest Canada, *Geology*, *12*, 68–72.

Housh, T., S. A. Bowring, and M. Villeneuve (1989), Lead isotopic study of early Proterozoic Wopmay orogen, NW Canada: Role of continental crust in arc magmatism, *Geol. J.*, *97*, 735–747.

Jackson, V. A. (2006), Preliminary geologic map of part of the southern Wopmay orogen (parts of NTS 86B and 86C), *Northwest Territories Geoscience Office, NWT Open Rep. 2006-004*, *1 Map*, scale 1:100,000, and accompanying report, 41 pp.

Jones, A. G. (1983), On the equivalence of the "Niblett" and "Bostick" transformations in the magnetotelluric method, *J. Geophys.*, *53*, 72–73.

Jones, A. G. (1992), Electrical conductivity of the continental lower crust, in *Continental Lower Crust*, edited by D. M. Fountain, R. J. Arculus, and R. W. Kay, pp. 81–143, Elsevier, New York.

Jones, A. G. (1999), Imaging the continental upper mantle using electromagnetic methods, *Lithos*, *48*, 57–80.

Jones, A. G. (2006), Electromagnetic interrogation of the anisotropic Earth: Looking into the Earth with polarized spectacles, *Phys. Earth Planet. Inter.*, *158*, 281–291.

Jones, A. G., and H. Jödicke (1984), Magnetotelluric transfer function estimation improvement by a coherence-based rejection technique, paper presented at the 54th Society of Exploration Geophysics Annual General Meeting, Atlanta, Georgia, 2–6 December, Abstract volume, pp. 51–55.

Jones, A. G., and J. A. Craven (1990), The North American Central Plains conductivity anomaly and its correlation with gravity, magnetic, seismic and heat flow data in Saskatchewan, Canada, *Phys. Earth Planet. Inter.*, *60*, 169–194.

Jones, A. G., and R. W. Groom (1993), Strike angle determination from the magnetotelluric tensor in the presence of noise and local distortion: Rotate at your peril!, *Geophys. J. Int.*, *113*, 524–534.

Jones, A. G., and I. J. Ferguson (2001), The electric Moho, *Nature*, *409*, 331–333.

Jones, A. G., and J. Spratt (2001), A simple method for deriving the uniform field MT responses in auroral zones, *Earth Planet. Sci. Lett.*, *54*, 443–450.

Jones, A. G., and J. A. Craven (2004), Area selected for diamond exploration using deep-probing electromagnetic surveying, *Lithos*, *71*, 765–782.

Jones, A. G., and X. Garcia (2006), Electrical resistivity structure of the Yellowknife River fault zone and surrounding region, in *Gold in the Yellowknife Greenstone Belt, Northwest Territories: Results of the EXTECH III Multidisciplinary Research Project*, edited by C. D. Anglin et al., *Geol. Assoc. of Can. Miner. Deposits Div. Spec. Publ.*, *3*, 126–141.

Jones, A. G., A. D. Chave, G. D. Egbert, D. Auld, and K. Bahr (1989), A comparison of techniques for magnetotelluric response function estimation, *J. Geophys. Res.*, *94*, 14,201–14,213.

Jones, A. G., R. D. Kurtz, D. E. Boerner, J. A. Craven, G. W. McNeice, D. I. Gough, J. M. De Laurier, and R. G. Ellis (1992), Electromagnetic constraints on strike-slip fault geometry; the Fraser River fault system, *Geology*, *20*, 561–564.

Jones, A. G., J. Katsube, and P. Schwann (1997), The longest conductivity anomaly in the world explained: Sulfides in fold hinges causing very high electrical anisotropy, *J. Geomagn. Geoelectr.*, *49*, 1619–1627.

Jones, A. G., I. J. Ferguson, A. D. Chave, R. L. Evans, and G. W. McNeice (2001), The electric lithosphere of the Slave craton, *Geology*, *29*, 423–426.

Jones, A. G., D. Snyder, S. Hanmer, I. Asudeh, and D. White (2002), Magnetotelluric and teleseismic study across the Snowbird tectonic zone, Canadian Shield: A Neoarchean mantle suture?, *Geophys. Res. Lett.*, *29*(17), 1829, doi:10.1029/2002GL015359.

Jones, A. G., P. Lezaeta, I. J. Ferguson, A. D. Chave, R. L. Evans, X. Garcia, and J. Spratt (2003), The electrical structure of the Slave craton, *Lithos*, *71*, 505–527.

Jones, A. G., J. Ledo, and I. J. Ferguson (2005), Electromagnetic images of the Trans-Hudson orogen: The North American Central Plains anomaly revealed, *Can. J. Earth Sci.*, *42*, 457–478.

Karato, S. (1990), The role of hydrogen in the electrical conductivity of the upper mantle, *Nature*, *347*, 272–273.

Katsube, T. J., J. Kerswill, S. Connell, P. Keating, H. Falck, and N. Scromeda-Perez (2006), Geophysical and petrophysical characteristics of host rocks, alteration zones and structures associated with gold mineralization in the Yellowknife mining district, in *Gold in the Yellowknife Greenstone Belt, Northwest Territories: Results of the EXTECH III Multidisciplinary Research Project*, *Geol. Assoc. of Can. Miner. Deposits Div. Spec. Publ. 3*, chap. 21, 325–339.

Kopylova, M. G., and G. Caro (2004), Mantle xenoliths from the Southeastern Slave craton: The evidence for a thick cold stratified lithosphere, *J. Petrol.*, *45*, 1045–1067.

Kopylova, M. G., J. K. Russell, and H. Cookenboo (1999), Petrology of peridotite and pyroxenite xenoliths from the Jericho kimberlite: Implications for the thermal state of the mantle beneath the Slave craton, Northern Canada, *J. Petrol.*, *40*, 79–104.

Lawrence, B. A., M. Pilkington, and F. M. Warner (2003), Interpretations of Precambrian basement based on recent aeromagetic data, Mackenzie Valley, Northwest Territories, *Geol. Surv. of Can., Curr. Res., 2003-C2*, 11 pp.

Ledo, J., and A. G. Jones (2005), Temperature of the upper mantle beneath the Intermontane Belt, northern Canadian Cordillera, determined from combining mineral composition, electrical conductivity laboratory studies and magnetotelluric field observations, *Earth Planet. Sci. Lett.*, *236*, 258–268.

Mackie, R. L., and T. R. Madden (1993), Three-dimensional magnetotelluric inversion using conjugate gradients, *Geophys. J. Int.*, *115*, 215–229.

Mareschal, M. (1986), Modeling of natural sources of magnetospheric origin in the interpretation of regional induction studies: A review, *Surv. Geophys.*, *8*, 261–300.

Mareschal, M., R. L. Kellett, R. D. Kurtz, J. N. Ludden, and R. C. Bailey (1995), Archean cratonic roots, mantle shear zones and deep electrical anisotropy, *Nature*, *375*, 134–137.

Mareschal, J. C., A. Nyblade, H. K. C. Perry, C. Jaupart, and G. Bienfait (2004), Heat flow and deep lithospheric thermal structure at Lac de Gras, Slave Province, Canada, *Geophys. Res. Lett.*, *31*, L12611, doi:10.1029/2004GL020133.

McNeice, G. W., and A. G. Jones (2001), Multisite, multifrequency tensor decomposition of magnetotelluric data, *Geophysics*, *66*, 158–173.

Mibe, K., T. Fujii, and A. Yasuda (1998), Connectivity of aqueous fluid in the Earth's upper mantle, *Geophys. Res. Lett.*, *25*, 1233–1236.

Narod, B. B., and J. R. Bennest (1990), Ring-core fluxgate magnetometers for use as observatory variometers, *Phys. Earth Planet. Inter.*, *59*, 23–28.

Nesbitt, B. E. (1993), Electrical resistivities of crustal fluids, *J. Geophys. Res.*, *98*, 4301–4310.

Ootes, L., and K. Pierce (2005), A digital geological atlas of the Wecho River area, *Northwest Territories Geoscience Office, NWT Open File 2005-03*, 1 [CD-ROM].

Partzsch, G. M., F. R. Schilling, and J. Arndt (2000), The influence of partial melting on the electrical behaviour of crustal rocks: Laboratory examination, model calculations and geological interpretations, *Tectonophysics*, *317*, 189–203.

Pearson, N. J., W. L. Griffin, B. J. Doyle, S. Y. O'Reilly, E. Van Achterbergh, and K. Kivi (1999), Xenoliths from kimberlite pipes of the Lac de Gras area, Slave craton, Canada, in *Proceedings of the 7th International Kimberlite Conference*, vol. 2, edited by J. J. Gurney et al., pp. 644–658, P.H. Nixon Volume, Red Roof Design, Cape Town.

Pierce, K. L., and W. A. Turner (2004), GIS compilation of the southern Wopmay orogen (south of 65°N), *Northwest Territories Geoscience Office, NWT Open Rep. 2004–005*, 1 [CD-ROM].

Rankin, D. (1962), The magneto-telluric effect on a dike, *Geophysics*, *27*, 666–676.

Ritter, O., A. Hoffmann-Rothe, P. Bedrosian, U. Weckman, and V. Haak (2005), Electrical conductivity images of active and fossil fault zones, *Geol. Soc. Spec. Publ.*, *245*, 165–186.

Roberts, J. J., A. G. Duba, E. A. Mathez, T. J. Shankland, and R. Kinzler (1999), Carbon-enhanced electrical conductivity during fracture of rocks, *J. Geophys. Res.*, *104*, 737–747.

Rodi, W., and R. L. Mackie (2001), Nonlinear conjugate gradients algorithm for 2-D magnetotelluric inversion, *Geophysics*, *66*, 174–186.

Schmucker, U. (1970), *Anomalies of Geomagnetic Variations in the South-Western United States*, *Bull. Scripps Inst. Ocean.*, vol. 13, 165 pp., Univ. Calif. Press.

Snyder, D. B. (2008), Stacked uppermost mantle layers within the Slave craton of NW Canada as defined by anisotropic seismic discontinuities, *Tectonics*, *27*, TC4006, doi:10.1029/2007TC002132.

Snyder, D. B., and M. Bruneton (2007), Seismic anisotropy of the Slave craton, NW Canada, from joint interpretation of SKS and Rayleigh waves, *Geophys. J. Int.*, *169*, 170–188, doi:10.1111/j.1365-246X.2006.03287.x.

Snyder, D. B., M. Bostock, and G. D. Lockhart (2003), Two anisotropic layers in the Slave craton, *Lithos*, *71*, 529–539.

Solon, K., A. G. Jones, K. D. Nelson, M. J. Unsworth, and the INDEPTH MT team (2005), Structure of the crust in the vicinity of the Banggong-Nujiang suture central Tibet from INDEPTH magnetotelluric data, *J. Geophys. Res.*, *110*, B10102, doi:10.1029/2003JB002405.

Stubley, M. P. (2005), Slave craton: Interpretive bedrock compilation, *Northwest Territories Geoscience Office, NWT Open File Rep. 2005-01*.

Ten Grotenhuis, S. M., M. R. Drury, C. J. Peach, and C. J. Spiers (2004), Electrical properties of fine-grained olivine: Evidence for grain boundary transport, *J. Geophys. Res.*, *109*, B06203, doi:10.1029/2003JB002799.

Thorpe, R. I., G. L. Cumming, and J. K. Mortensen (1992), A significant Pb isotope boundary in the Slave Province and its probable relation to ancient basement in the western Slave Province, *Geol. Surv. of Can. Open File Rep. 2484*, pp. 179–184.

Wait, J. R. (1962), Theory of magnetotelluric fields, *J. Res. Natl. Bur. Stand., D Radio Propag.*, *66d*, 509–541.

Wannamaker, P. E., G. R. Jiracek, J. A. Stodt, T. G. Caldwell, V. M. Gonzalez, D. McKnight, and A. D. Porter (2002), Fluid generation and pathways beneath an active compressional orogen, the New Zealand Southern Alps, inferred from magnetotelluric data, *J. Geophys. Res.*, *107*(B6), 2117, doi:10.1029/2001JB000186.

Wu, X., I. J. Ferguson, and A. G. Jones (2002), Magnetotelluric response and geoelectric structure of the Great Slave Lake shear zone, *Earth Planet. Sci. Lett.*, *196*, 35–50.

Wu, X., I. J. Ferguson, and A. G. Jones (2005), Geoelectric structure of the Proterozoic Wopmay orogen and adjacent terranes, Northwest Territories, Canada, *Can. J. Earth Sci.*, *42*, 1–27.

Xu, Y., T. J. Shankland, and B. T. Poe (2000), Laboratory-based electrical conductivity of the Earth's mantle, *J. Geophys. Res.*, *105*, 27,865–27,875.

A. Avdeeva, L. Collins, A. G. Jones, and J. E. Spratt, Dublin Institute for Advanced Studies, 5 Merrion Square, Dublin 2, Ireland. (aavdeeva@cp.dias.ie; lcollins@cp.dias.ie; alan@cp.dias.ie; jsp@cp.dias.ie)

V. A. Jackson, NWT Geoscience Office, Yellowknife, NT Canada X1A 2R3. (valerie_jackson@gov.nt.ca)